

Renormalization of the cyclic Wilson loop

Matthias Berwein,¹ Nora Brambilla,¹ Jacopo Ghiglieri,² and Antonio Vairo¹

¹*Physik-Department, Technische Universität München,
James-Frank-Str. 1, 85748 Garching, Germany*

²*McGill University, Department of Physics,
3600 rue University, Montreal QC H3A 2T8, Canada*

E-mail: matthias.berwein@mytum.de, nora.brambilla@tum.de,
jacopo.ghiglieri@physics.mcgill.ca, antonio.vairo@tum.de

ABSTRACT: In finite-temperature field theory, the cyclic Wilson loop is defined as a rectangular Wilson loop spanning the whole compactified time direction. In a generic non-abelian gauge theory, we calculate the perturbative expansion of the cyclic Wilson loop up to order g^4 . At this order and after charge renormalization, the cyclic Wilson loop is known to be ultraviolet divergent. We show that the divergence is not associated with cusps in the contour but is instead due to the contour intersecting itself because of the periodic boundary conditions. One consequence of this is that the cyclic Wilson loop mixes under renormalization with the correlator of two Polyakov loops. The resulting renormalization equation is tested up to order g^6 and used to resum the leading logarithms associated with the intersection divergence. Implications for lattice studies of this operator, which may be relevant for the phenomenology of quarkonium at finite temperature, are discussed.

KEYWORDS: Wilson loop, renormalization, cusp divergences, intersections, periodic boundary conditions

Contents

1	Introduction	1
2	Definition and properties of the cyclic Wilson loop	2
3	The cyclic Wilson loop at short distances up to $\mathcal{O}(\alpha_s^2)$	7
4	Renormalization	11
4.1	The cyclic Wilson loop at short distances at leading logarithmic accuracy	16
5	Renormalization up to $\mathcal{O}(\alpha_s^3)$	16
5.1	Divergences	17
5.2	Renormalization	20
6	The cyclic Wilson loop at large distances	26
7	Conclusions	27

1 Introduction

Wilson loops, ever since their introduction [1], have been an important tool in the study of non-abelian gauge theories. In particular, rectangular loops with one spatial and one time direction, also known as static Wilson loops, have played a crucial role in the understanding of QCD, for their Coulomb-like behaviour at short distances is a manifestation of asymptotic freedom and their area-law behaviour at large distances of confinement. Since static Wilson loops in the large time limit are related to the energy of a static quark-antiquark pair [2, 3], static Wilson loops are also important quantities for quarkonium studies [4–6].

At finite temperature, because quarkonium dissociation provides a probe of the properties of the QCD medium created in heavy-ion collisions [7], Wilson loops and other observables related to Wilson lines have been widely used and measured on the lattice (see [8] for a review). The periodic boundary conditions that characterize the fields in a thermal field theory allow indeed for the definition of other gauge-invariant operators besides the Wilson loop. An example is the trace of the Polyakov loop, i.e. a Wilson line spanning the entire compactified time axis, and correlators thereof. Gauge-dependent quantities, such as the trace of the product of two Polyakov loops, have also been studied.

In this paper, we focus on the *cyclic Wilson loop*, i.e. a rectangular Wilson loop whose time extent spans the entire Euclidean time axis, i.e. from 0 to $1/T$, where T is the temperature. This quantity can be seen as a gauge-invariant completion of the aforementioned product of two Polyakov loops. In particular, we study its renormalization. The motivation for this study comes from Ref. [9], where an order g^4 perturbative calculation in

dimensional regularization showed that the thermal expectation value of the cyclic Wilson loop is ultraviolet (UV) divergent after charge renormalization.

It is known that a smooth Wilson loop is finite after charge renormalization in dimensional regularization [10, 11]. If the contour has cusps, additional UV divergences occur. These divergences are called *cusp divergences* and the coefficients multiplying them, and hence their anomalous dimensions, depend only on the angle at the cusp. Such divergences are renormalized through a multiplicative constant. This constant and the associated *cusp anomalous dimension* are known to two loops in QCD [12] and to three loops in $\mathcal{N} = 4$ supersymmetric Yang–Mills theory [13]. Furthermore, in [14], the *intersection divergence*, i.e. a UV divergence arising from an otherwise smooth contour intersecting itself, was first considered; it was shown that its renormalization is nontrivial and mixes all possible loops and correlators of loops sharing the same geometry.

In this paper, we will show that the divergence appearing in the cyclic loop is an intersection divergence, the intersection being caused by the periodic boundary conditions. The renormalization equation mixes the cyclic Wilson loop with the correlator of two Polyakov loops. This equation holds to all orders. We will explicitly check this up to order g^6 . Furthermore, the related renormalization group equations allow to resum logarithms associated with the intersection divergence; we will explicitly provide the resummed expression valid at leading logarithmic accuracy.

The paper is organized as follows. In Sec. 2, we introduce some properties of Wilson loops and cyclic Wilson loops that will be relevant for the rest of the paper. In Sec. 3, we compute the cyclic loop at order g^4 at short distances $r \ll 1/T$. Our result, UV divergence included, reproduces the short-distance limit of a calculation first presented in [9]. In Sec. 4, we introduce the renormalization of intersection divergences derived in [14] and apply it to the cyclic Wilson loop, obtaining its renormalization equation. The perturbative expression of the cyclic Wilson loop is used to determine the order g^2 contribution to the renormalization constant appearing in the renormalization equation. The renormalization-group equation is solved at leading logarithmic accuracy. In Sec. 5, we examine the structure of intersection divergences up to order g^6 ; we show how our equation correctly cancels these divergences, providing a non-trivial test of the renormalization equation. In Sec. 6, we show that the same equation that renormalizes the cyclic Wilson loop at short distances renormalizes it at long distances. Our expression for the UV divergence at long distance disagrees with the corresponding one that can be found in [9]; we analyze the origin of the disagreement. Finally, in Sec. 7, we draw our conclusions, emphasizing the relevance of the result for a proper lattice evaluation of the cyclic Wilson loop. Some of the results presented here can be found in [15].

2 Definition and properties of the cyclic Wilson loop

Before we turn to the issue of the renormalization of the cyclic Wilson loop, we will start by giving some general properties that will be instrumental in the following discussion. In Euclidean spacetime, the cyclic Wilson loop, W_c , is defined as the product of four straight Wilson lines, U , two of which extend in the time direction from 0 to $1/T$ while the other

two stretch in the spatial direction \mathbf{r} from $-\mathbf{r}/2$ to $\mathbf{r}/2$:¹

$$W_c = \left\langle \widetilde{\text{Tr}} \left[U_0 \left(\frac{\mathbf{r}}{2}, -\frac{\mathbf{r}}{2} \right) U_{-\frac{\mathbf{r}}{2}} (0, 1/T) U_{1/T} \left(-\frac{\mathbf{r}}{2}, \frac{\mathbf{r}}{2} \right) U_{\frac{\mathbf{r}}{2}} (1/T, 0) \right] \right\rangle, \quad (2.1)$$

where $\langle O \rangle$ stands for the thermal average of the operator O . The Wilson lines, U , are defined as

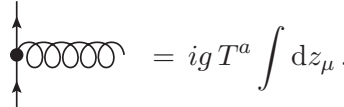
$$U_\tau \left(\frac{\mathbf{r}}{2}, -\frac{\mathbf{r}}{2} \right) = \mathcal{P} \exp \left[ig \int_0^1 ds \, \mathbf{r} \cdot \mathbf{A} \left(\left(s - \frac{1}{2} \right) \mathbf{r}, \tau \right) \right],$$

$$U_{\frac{\mathbf{r}}{2}} (\tau_2, \tau_1) = \mathcal{P} \exp \left[ig \int_{\tau_1}^{\tau_2} d\tau \, A_0 \left(\frac{\mathbf{r}}{2}, \tau \right) \right], \quad (2.2)$$

where $A_\mu = A_\mu^a T^a$ is the gluon field in Euclidean spacetime with boundary condition $A_\mu(\mathbf{r}, \tau + 1/T) = A_\mu(\mathbf{r}, \tau)$, \mathcal{P} stands for path ordering of the colour matrices and $\widetilde{\text{Tr}}$ denotes the trace in colour space divided by the number of colours N_c .² The four Wilson lines together give a rectangular path with sides $1/T$ and r . If we expand the cyclic Wilson loop in the coupling g and take heed of the path-ordering prescription, we get

$$W_c = \left\langle \widetilde{\text{Tr}} \left[\sum_{n=0}^{\infty} (ig)^n \oint dz_{1\mu} A_\mu(z_1) \oint^{z_1} dz_{2\nu} A_\nu(z_2) \cdots \oint^{z_{n-1}} dz_{n\rho} A_\rho(z_n) \right] \right\rangle. \quad (2.3)$$

The integral $\oint^{z_i} dz_{i+1\mu}$ is performed along the rectangular path and ends at the point z_i as a consequence of the path-ordering prescription for the colour matrices. Note that the gauge fields are instead time ordered [3]. The thermal average (2.3) is a series of Feynman diagrams each of them characterized by n external points z_i lying on the contour of the rectangular path over which we integrate according to the path-ordering prescription. Sticking to the terminology found e.g. in Ref. [16], it is convenient to refer to these external points, each one of which gets a factor ig , as *line vertices*, as opposed to *internal vertices* connecting gluons to other gluons, ghosts or light quarks. The corresponding Feynman rule for line vertices reads



$$= ig T^a \int dz_\mu. \quad (2.4)$$

Figure 1 shows all order α_s diagrams that can in principle contribute to the cyclic Wilson loop.³ They represent the first non-trivial contribution in the perturbative series:

$$W_c^{\mathcal{O}(\alpha_s)} = (ig)^2 C_F \oint dz_{1\mu} \oint^{z_1} dz_{2\nu} D_{\mu\nu}(z_1, z_2), \quad (2.5)$$

where $C_F = \widetilde{\text{Tr}}[T^a T^a] = (N_c^2 - 1)/(2N_c)$ is the quadratic Casimir in the fundamental representation.

¹Throughout the paper boldface characters will refer to three-vectors and italic characters to their modulus, e.g. $r \equiv |\mathbf{r}|$.

² We are working with the generators T^a in $A_\mu = A_\mu^a T^a$ in the fundamental representation of $SU(N_c)$.

³ This is the case for gauges in which $D_{0i} = 0$, such as the Feynman or Coulomb gauges. In a generic gauge, there would be also four extra diagrams where the gluon connects temporal with spatial lines.

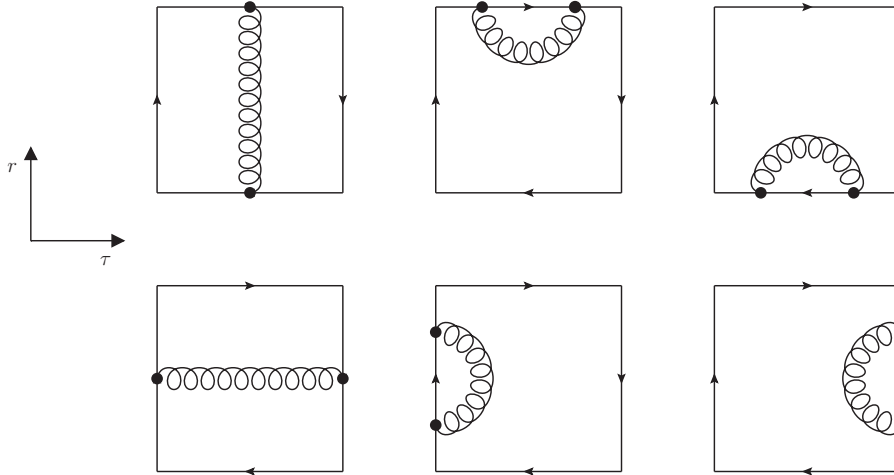


Figure 1. Diagrams that can in principle contribute at order α_s to the cyclic Wilson loop in gauges where $D_{0i} = 0$. The time, τ , runs along the horizontal axis and the spatial direction \mathbf{r} along the vertical axis.

It has been shown in Refs. [17] and [18] that the perturbative series for a Wilson loop can be rearranged and exponentiated as

$$W_c = \sum_{\gamma} C(\gamma)W(\gamma) = \exp \left[\sum_{\gamma \in 2\text{PI}} \tilde{C}(\gamma)W(\gamma) \right], \quad (2.6)$$

where $W(\gamma)$ stands for the value of a diagram γ without its *colour factor* given by $C(\gamma)$; $C(\gamma)$ is the trace divided by N_c of all colour matrices, T^a , contracted with all colour structure constants appearing in the diagram γ . Equation (2.6) states that the sum over all diagrams can be exponentiated in such a way that the exponent contains the sum over a subset of these diagrams only, called *two-particle irreducible* (2PI) diagrams. However, the colour factors of the diagrams in the exponent have to be replaced by new factors $\tilde{C}(\gamma)$. These factors are called *colour-connected* [18] or *maximally non-abelian* coefficients [17]. We will stick to the former expression and give an explicit definition below.

The term two-particle irreducible was coined after the one-particle irreducible diagrams that occur e.g. in the resummation of the geometric series of self-energy diagrams for the full propagator (indeed, Ref. [16] uses the expression one-particle irreducible, but we will stick to the terminology found e.g. in Ref. [12]). Here “particle” refers to the contour only: if it can be cut in two places in such a way that the resulting pieces are not connected through gluons, then such a diagram is reducible. If there is no possible way to cut the contour twice that leads to two disconnected pieces, then such a diagram is called irreducible. This is shown in Fig. 2. The first diagram is reducible, because if cut as indicated, the two resulting pieces do not exchange gluons between themselves. These two pieces are given schematically on the right, dropping all specifics of the contour except for how the gluons are attached to it. The diagram shown in the second and third line cannot be separated like the first diagram, regardless of how it is cut. All possibilities reduce to one of the two

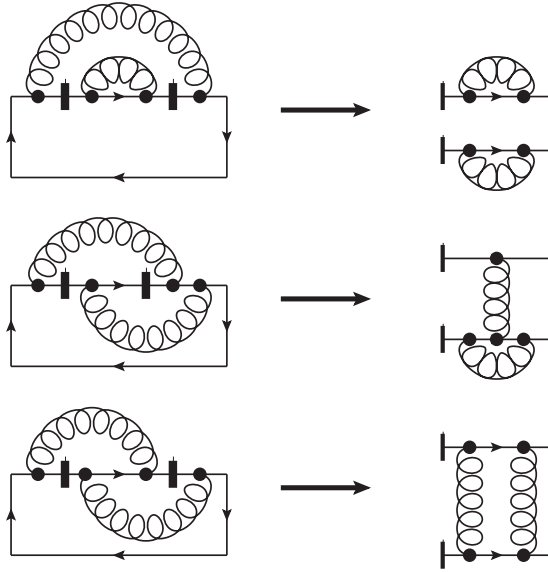


Figure 2. Example of a two-particle reducible (top) and an irreducible diagram (center and bottom).

cases shown. Of course, if one would cut out a piece without any gluons attached to it, then every diagram would be reducible making this definition meaningless, so this trivial case is excluded. Sometimes 2PI diagrams are also called rainbow irreducible (cf. Ref. [12]).

For further use it will be convenient to call a diagram *connected*, if every line vertex is connected to every other line vertex through gluons, internal vertices and possibly loops of quarks, gluons and ghosts, otherwise it will be called *unconnected*. Connected diagrams are irreducible, while unconnected diagrams, like those in Fig. 2, may or may not be reducible.

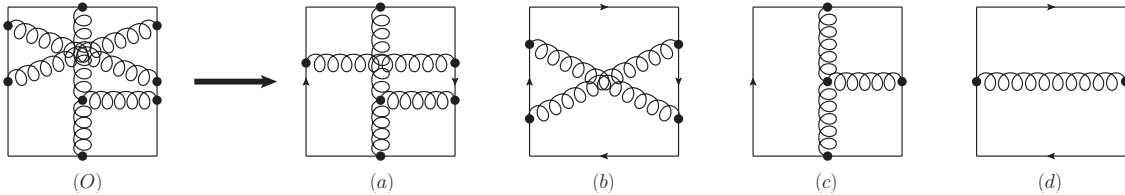


Figure 3. A list of all subdiagrams (called γ_a etc.) obtained from the diagram on the left γ_O .

With this terminology we can give a recursive definition of the colour-connected coefficients. For a connected diagram, the colour-connected coefficient is equal to its colour factor. We can think of unconnected diagrams as combinations of connected parts. By combining two diagrams we mean putting their line vertices on the same contour. A *subdiagram* of a given diagram can be obtained by removing any number of its connected parts. An example is given in Fig. 3: the four diagrams to the right represent all subdiagrams of the original diagram γ_O , obtained by removing one (in γ_a and γ_b) or two (in γ_c and γ_d) of the connected parts. In general there are several possible sets of subdiagrams that can be combined to form the original diagram. In our example these are $\{\gamma_a, \gamma_d\}$, $\{\gamma_b, \gamma_c\}$

and $\{\gamma_c, \gamma_d, \gamma_d\}$. In order to obtain the colour-connected coefficient for an unconnected diagram we need to take the products of colour-connected coefficients of the subdiagrams for each of these sets and subtract them from the colour factor of the original diagram. If there are several ways of combining the subdiagrams to form the original diagram, then the product of colour-connected coefficients needs to be multiplied by the number of possible combinations. For example, there are two ways to combine subdiagrams γ_a and γ_d : the left line vertex of γ_d can be put above or below the left line vertex of γ_a ; the same applies for the combination of $\{\gamma_c, \gamma_d, \gamma_d\}$. If a subdiagram appears n times in a set, then the corresponding product needs to be divided by $n!$. In our example the colour-connected coefficient is therefore given by

$$\tilde{C}(\gamma_O) = C(\gamma_O) - 2\tilde{C}(\gamma_a)\tilde{C}(\gamma_d) - \tilde{C}(\gamma_b)\tilde{C}(\gamma_c) - \frac{2}{2!}\tilde{C}(\gamma_c)\left(\tilde{C}(\gamma_d)\right)^2. \quad (2.7)$$

The colour-connected coefficients of unconnected subdiagrams can be obtained by recursive application of this definition. The recursion ends when there are only connected subdiagrams involved. So e.g. for γ_a we have

$$\tilde{C}(\gamma_a) = C(\gamma_a) - \tilde{C}(\gamma_c)\tilde{C}(\gamma_d) = C(\gamma_a) - C(\gamma_c)C(\gamma_d). \quad (2.8)$$

Although the definition does not require subdiagrams to be 2PI, we may neglect reducible subdiagrams in the calculation of colour-connected coefficients, since their colour-connected coefficients are zero.

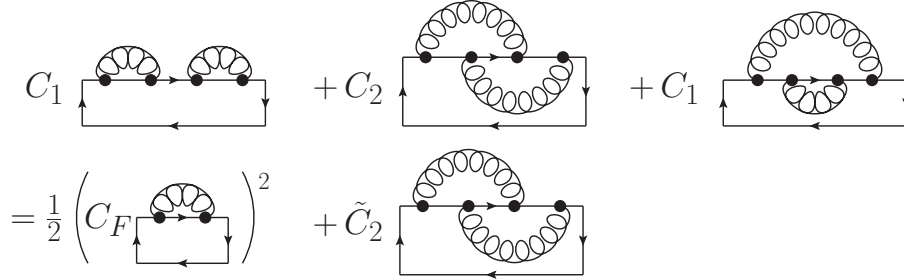


Figure 4. Example of exponentiation; C_F and $\tilde{C}_2 = -C_F C_A/2$ are colour-connected coefficients.

An illustration for Eq. (2.6) is given in Fig. 4. It shows a series of unconnected diagrams at $\mathcal{O}(\alpha_s^2)$ with the colour factors written explicitly in front of each diagram. We have

$$C_1 = \widetilde{\text{Tr}} \left[T^a T^a T^b T^b \right] = C_F^2 \quad \text{and} \quad C_2 = \widetilde{\text{Tr}} \left[T^a T^b T^a T^b \right] = C_F^2 - \frac{C_F C_A}{2}, \quad (2.9)$$

where $C_A = N_c$ is the quadratic Casimir of the adjoint representation. The first and last diagrams are reducible, the one in the middle is 2PI and its colour-connected coefficient is given by $\tilde{C}_2 = C_2 - 2C_F^2/2! = -C_F C_A/2$, since C_F is the colour-connected coefficient of a one-gluon diagram. The sum over the parts proportional to C_F^2 of all three diagrams gives the first term in the second line of Fig. 4, which we interpret as the second-order expansion of the exponential of the $\mathcal{O}(\alpha_s)$ diagram, while the remaining 2PI diagram with its modified coefficient is interpreted as a term from the first-order expansion.

The exponentiation theorem greatly reduces the number of diagrams that we need to consider when calculating a Wilson loop, for we just need to consider 2PI diagrams.⁴ For the cyclic Wilson loop, we can neglect yet another group of diagrams. As Eq. (2.2) shows, Wilson lines are unitary operators, whose inverse is given by an otherwise identical Wilson line but with the direction of the contour integration reversed. Hence we can rewrite the cyclic Wilson loop as

$$W_c = \left\langle \widetilde{\text{Tr}} \left[U_0 \left(\frac{\mathbf{r}}{2}, -\frac{\mathbf{r}}{2} \right) U_{-\frac{\mathbf{r}}{2}}^\dagger (1/T, 0) U_{1/T}^\dagger \left(\frac{\mathbf{r}}{2}, -\frac{\mathbf{r}}{2} \right) U_{\frac{\mathbf{r}}{2}} (1/T, 0) \right] \right\rangle. \quad (2.10)$$

Wilson lines going from 0 to $1/T$ on the time axis are Polyakov loop operators. Because they are related to the free energy of an infinitely heavy quark in the thermal medium [19], we will refer to them as *quark lines*. The other two Wilson lines will be called *strings*, because they act as gauge links between the two Polyakov loop operators. We will use the terms quark line and string to denote both the operators and the corresponding contours in spacetime. Because of the periodic boundary conditions on the Euclidean time, the two strings are at the same position and can be seen to combine into an adjoint Wilson line. If we expand one of the quark lines to zeroth order in α_s then the strings cancel:

$$\begin{aligned} W_c &= \left\langle \widetilde{\text{Tr}} \left[U_0 \left(\frac{\mathbf{r}}{2}, -\frac{\mathbf{r}}{2} \right) U_{-\frac{\mathbf{r}}{2}}^\dagger (1/T, 0) U_{1/T}^\dagger \left(\frac{\mathbf{r}}{2}, -\frac{\mathbf{r}}{2} \right) U_{\frac{\mathbf{r}}{2}} (1/T, 0) \right] \right\rangle \\ &= \left\langle \widetilde{\text{Tr}} \left[U_0 \left(\frac{\mathbf{r}}{2}, -\frac{\mathbf{r}}{2} \right) (\mathbb{I} + \dots) U_0^\dagger \left(\frac{\mathbf{r}}{2}, -\frac{\mathbf{r}}{2} \right) U_{\frac{\mathbf{r}}{2}} (1/T, 0) \right] \right\rangle \\ &= \left\langle \widetilde{\text{Tr}} \left[U_{\frac{\mathbf{r}}{2}} (1/T, 0) \right] \right\rangle + \dots \end{aligned} \quad (2.11)$$

In terms of diagrams, the zeroth-order expansion of a quark line corresponds to diagrams without any line vertices on that quark line. Equation (2.11) shows that in this case all diagrams with line vertices on the strings cancel against each other and what is left is a Polyakov loop. As the second line of the equation shows, this cancellation happens at any order in perturbation theory whenever the colour-singlet component of either of the two quark lines is considered. Some examples are given for illustrative purposes in Fig. 5. This leaves only diagrams with all line vertices on the same quark line or diagrams with some line vertices on both quark lines. Line vertices on the strings contribute only in the latter case. Because this cancellation is directly linked to the periodic boundary conditions and to the fact that the cyclic Wilson loop spans the entire compactified time axis, we will call it *cyclicity cancellation*.

3 The cyclic Wilson loop at short distances up to $\mathcal{O}(\alpha_s^2)$

Having illustrated some general properties of the cyclic Wilson loop, exponentiation and cyclicity cancellation, we can now turn to its calculation up to order g^4 . In particular, we will investigate UV divergences. The analysis of this section will be extended up to order g^6 in Sec. 5.

⁴We remark that in an abelian theory all colour factors are one and only connected diagrams contribute to the exponent of Eq. (2.6).

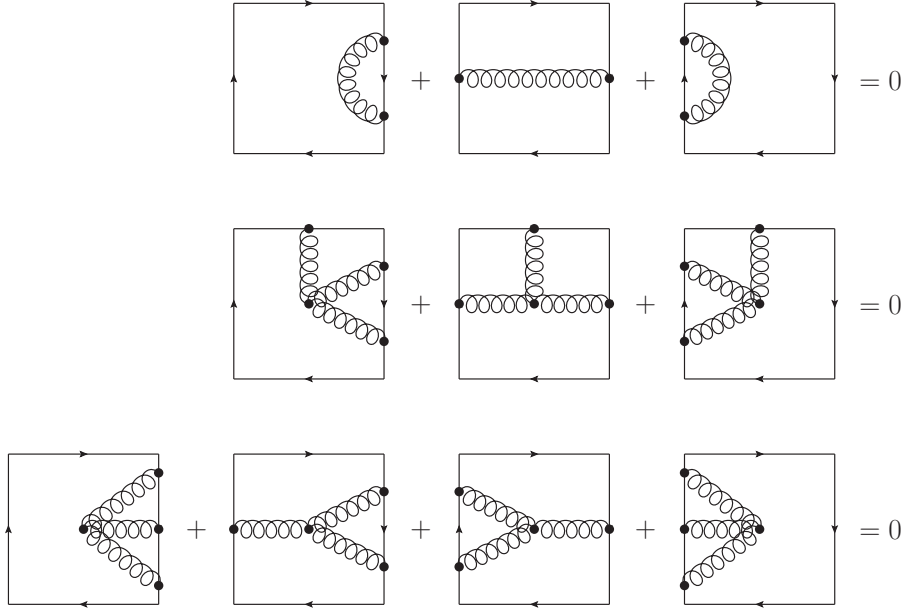


Figure 5. Diagrams canceling because of cyclicity.

The cyclic Wilson loop is a thermal average, therefore, besides the scale $1/r$ that characterizes the correlation of two quark lines at a distance r , it depends on the temperature T . We will assume that these scales are much larger than the confinement scale, so that their contribution may be computed in perturbation theory. Other scales are also relevant: the in vacuum static energy, which in a weak-coupling regime is proportional to α_s/r and the screening or Debye mass m_D , which in a weak-coupling regime is proportional to gT . In order to be definite, we will assume $1/r \gg T \gg m_D \gg \alpha_s/r$. The reason for this choice is that the same hierarchy was assumed for the correlator of two Polyakov loops in [20] and we will need the expression of the correlator of two Polyakov loops for renormalizing the cyclic Wilson loop at order g^6 .

The cyclic Wilson loop is gauge invariant, so the choice of the gauge in which to perform the calculation is only a matter of convenience. A convenient gauge is the Coulomb gauge that we will adopt in this section if not stated otherwise, whereas the analysis of Sec. 5 will not rely on a specific gauge choice.

The $\mathcal{O}(\alpha_s)$ diagrams are shown in Fig. 1. The diagrams in the second row cancel because of cyclicity (see also Fig. 5). In the first row, only the diagram on the left, where the gluon connects to both quark lines, contributes to the cyclic Wilson loop. The other two diagrams vanish in dimensional regularization. The reason is that the contour integration along the time axis, i.e. $\int_0^{1/T} d\tau e^{i\omega_n \tau}$ with $\omega_n = 2\pi nT$ the bosonic Matsubara frequencies, selects the zero mode $n = 0$, but then the remaining integration over the spatial momentum \mathbf{k} depends neither on r nor on T and vanishes in dimensional regularization for being scaleless. Contributions from the scale m_D are of higher order. This line of argument is gauge independent, so the fact that the only contributing diagram is the first diagram

on the left in Fig. 1 is a gauge-independent statement. The diagram gives

$$\ln W_c = \frac{C_F \alpha_s}{rT} + \mathcal{O}(\alpha_s^2) . \quad (3.1)$$

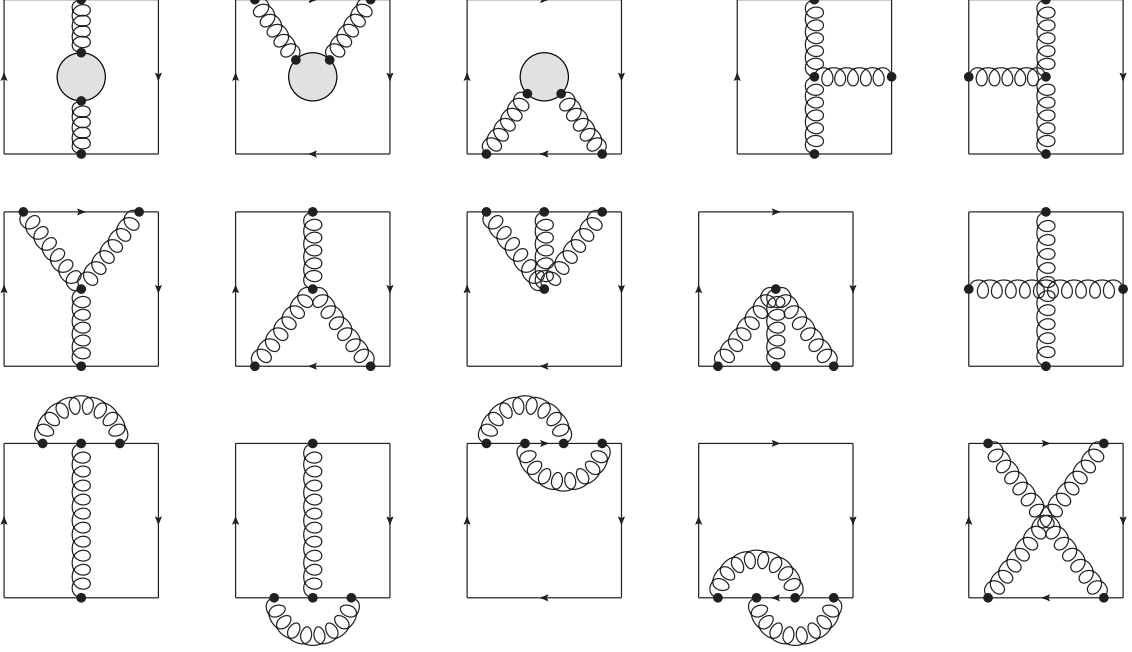


Figure 6. All relevant diagrams at $\mathcal{O}(\alpha_s^2)$. As in Fig. 1 we restrict ourselves to gauges where $D_{0i} = 0$.

At $\mathcal{O}(\alpha_s^2)$ all irreducible diagrams that do not cancel through cyclicity are shown in Fig. 6. The first three diagrams in the first row involve the gluon self-energy. This can be split up into a thermal and a vacuum part, where the thermal part is defined as the one depending on the Bose–Einstein or Fermi–Dirac distribution functions. In Coulomb gauge, the thermal part of the gluon self-energy at zero Matsubara frequency reads

$$\begin{aligned} \Pi_{00}^{(T)}(0, \mathbf{k}) = & \frac{4\alpha_s C_A}{\pi} \int_0^\infty dq q n_B(q) \left[1 - \frac{k^2}{2q^2} + \left(\frac{q}{k} - \frac{k}{2q} + \frac{k^3}{8q^3} \right) \ln \left| \frac{2q+k}{2q-k} \right| \right] \\ & + \frac{4\alpha_s n_f}{\pi} \int_0^\infty dq q n_F(q) \left[1 + \left(\frac{q}{k} - \frac{k}{4q} \right) \ln \left| \frac{2q+k}{2q-k} \right| \right] , \end{aligned} \quad (3.2)$$

where n_f is the number of massless fermions, and $n_B(q) = 1/(\exp(q/T) - 1)$ and $n_F(q) = 1/(\exp(q/T) + 1)$ are the Bose–Einstein and Fermi–Dirac distributions respectively. We have taken the zero Matsubara frequency because, as before, this is the only contribution that survives the time integration. The gauge contribution to (3.2) can be read from [21], whereas the fermionic contribution can be found in textbooks such as [22]. The expression of $\Pi_{00}^{(T)}(0, \mathbf{k})$ clearly shows that the thermal part of the self-energy is not UV divergent. Instead, all three diagrams that involve the gluon self-energy are IR divergent, but the IR divergences cancel each other [23]. Regarding the vacuum part of the gluon-self energy, its

expression in Coulomb gauge is known and can be read, for instance, from [24]. Summing together vacuum and thermal part, we get from the first three diagrams of Fig. 6

$$\begin{aligned} & \frac{C_F \alpha_s^2}{T} \int \frac{d^d k}{(2\pi)^d} \frac{e^{i\mathbf{r}\cdot\mathbf{k}}}{\mathbf{k}^2} \left[\left(\frac{31}{9} C_A - \frac{10}{9} n_f \right) + \beta_0 \left(\frac{1}{\varepsilon} + \ln 4\pi - \gamma_E - \ln \mathbf{k}^2 \right) \right] \\ & + \frac{4\pi C_F \alpha_s}{T} \int \frac{d^3 k}{(2\pi)^3} (e^{i\mathbf{r}\cdot\mathbf{k}} - 1) \left[\frac{1}{\mathbf{k}^2 + \Pi_{00}^{(T)}(0, \mathbf{k})} - \frac{1}{\mathbf{k}^2} \right], \end{aligned} \quad (3.3)$$

where $\beta_0 = 11C_A/3 - 2n_f/3$ and the first integral has been regularized in $d = 3 - 2\varepsilon$ dimensions. The integral $\int \frac{d^d k}{(2\pi)^d} \frac{e^{i\mathbf{r}\cdot\mathbf{k}}}{\mathbf{k}^2}$ gives $\frac{1}{4\pi r} + \mathcal{O}(\varepsilon)$, but, since the $\mathcal{O}(\varepsilon)$ term multiplies a $1/\varepsilon$ pole, we leave it uncomputed for the time being. The first line is the vacuum part and reproduces the well-known one-loop contribution to the $Q\bar{Q}$ static potential [25, 26]. The UV divergence in the vacuum part can be removed by charge renormalization. In the second line, the term in square brackets simplifies to $-\Pi_{00}^{(T)}(0, \mathbf{k})/\mathbf{k}^4$ when k is integrated over the momentum regions $k \sim 1/r$ and $k \sim T$, whereas the part of $\Pi_{00}^{(T)}(0, \mathbf{k})$ of order m_D^2 has to be kept unexpanded when integrating over the momentum region $k \sim m_D$.

The other two diagrams in the first row of Fig. 6 are finite; each contributes $C_F C_A \alpha_s^2/2$. The first four diagrams in the second row give zero, because in gauges where time and space components do not mix, the three-gluon vertex for three longitudinal gluons vanishes. Also all five diagrams in the third row vanish in Coulomb gauge: the first four, because they involve scaleless integrals, and the last one because it is proportional to a function with vanishing support along the time axis.

The last diagram in the second row, however, does give a contribution, which is ultra-violet divergent even after charge renormalization. The divergence comes from the vacuum part of the gluon connecting the strings. The thermal part is finite and will be given as a series expansion in rT , which, according to our adopted hierarchy of energy scales, is a small parameter. The radius of convergence for this expansion is $rT \leq 1$. We obtain

$$\begin{aligned} & \frac{4C_F C_A \alpha_s^2}{T} \int \frac{d^d k}{(2\pi)^d} \frac{e^{i\mathbf{r}\cdot\mathbf{k}}}{\mathbf{k}^2} \left(\frac{1}{\varepsilon} + 1 + \gamma_E + \ln \pi + \ln r^2 \right) + \frac{2C_F C_A \alpha_s^2}{\pi} \sum_{n=1}^{\infty} \frac{(-1)^n \zeta(2n)}{n(4n^2 - 1)} (rT)^{2n-1}. \end{aligned} \quad (3.4)$$

The previous calculation shows the specific advantages of the Coulomb gauge: UV divergences related to charge renormalization occur only in diagrams with gluon self-energy insertions, the uncanceled extra divergence arises only from the last diagram in the second row of Fig. 6, and several diagrams vanish. For comparison, in Feynman gauge only the diagrams with a three-gluon vertex in the second row vanish, while the two diagrams on the left of the third row are also divergent and contribute to both the divergence that is removed by charge renormalization and the one which remains after that. Since the cyclic Wilson loop is gauge invariant, the complete expression up to $\mathcal{O}(\alpha_s^2)$ is the same for both

gauges (we have explicitly checked this) and reads

$$\begin{aligned}
\ln W_c = & \frac{C_F \alpha_s}{rT} \\
& + \frac{C_F \alpha_s^2}{T} \int \frac{d^d k}{(2\pi)^d} \frac{e^{i\mathbf{r} \cdot \mathbf{k}}}{\mathbf{k}^2} \left[\left(\frac{31}{9} C_A - \frac{10}{9} n_f \right) + \beta_0 \left(\frac{1}{\varepsilon} + \ln 4\pi - \gamma_E - \ln \mathbf{k}^2 \right) \right] \\
& + \frac{4\pi C_F \alpha_s}{T} \int \frac{d^3 k}{(2\pi)^3} \left(e^{i\mathbf{r} \cdot \mathbf{k}} - 1 \right) \left[\frac{1}{\mathbf{k}^2 + \Pi_{00}^{(T)}(0, \mathbf{k})} - \frac{1}{\mathbf{k}^2} \right] \\
& + \frac{2C_F C_A \alpha_s^2}{\pi} \sum_{n=1}^{\infty} \frac{(-1)^n \zeta(2n)}{n(4n^2 - 1)} (rT)^{2n-1} + C_F C_A \alpha_s^2 \\
& + \frac{4C_F C_A \alpha_s^2}{T} \int \frac{d^d k}{(2\pi)^d} \frac{e^{i\mathbf{r} \cdot \mathbf{k}}}{\mathbf{k}^2} \left(\frac{1}{\varepsilon} + 1 + \gamma_E + \ln \pi + \ln r^2 \right) + \mathcal{O}(g^5) , \tag{3.5}
\end{aligned}$$

with $\Pi_{00}^{(T)}(0, \mathbf{k})$ given by Eq. (3.2). Equation (3.5) agrees with the short-distance limit of the result that can be found in Ref. [9]; it thereby confirms their finding that the cyclic Wilson loop is not finite after charge renormalization.

The divergence in the second line of (3.5) can be removed by charge renormalization. The divergence coming from the last diagram in the second row of Fig. 6, whose analytical expression is in the $1/\varepsilon$ pole in the last line of (3.5), is very peculiar in that it is not of the form of a cusp divergence typically associated to a non-smooth Wilson loop. We recall that cusp divergences only depend on the angle γ at the cusp. In Euclidean spacetime, the leading-order divergence reads in dimensional regularization⁵ [12]

$$\frac{\alpha_s C_F}{2\pi\varepsilon} [1 + (\pi - \gamma) \cot \gamma] . \tag{3.6}$$

For four right angles, like in the case of a rectangular Wilson loop, Eq. (3.6) gives $2\alpha_s C_F/(\pi\varepsilon)$; this divergence, being independent on r and T , can be removed by a multiplicative factor. This is not the case for the divergence we are discussing here, which is of order α_s^2 and depends on the distance and on the temperature. In the next section, we will show how to properly renormalize this divergence.

4 Renormalization

In this section we will assume that charge renormalization has been carried out, so that we only need to concern ourselves with the remaining UV divergence in Eq. (3.5). This divergence is related to the specifics of the contour. Due to the periodic boundary conditions, the contour of a cyclic Wilson loop has support on a Euclidean cylindric space with d space dimensions extending from $-\infty$ to $+\infty$ and one compactified time dimension. Because the cyclic Wilson loop wraps around the full time dimension, the two strings run actually along the same line. This implies that the cyclic Wilson loop has no cusps, but only intersections, as shown in Fig. 7.

⁵The angular dependence in a cut-off regularization was derived in [10].

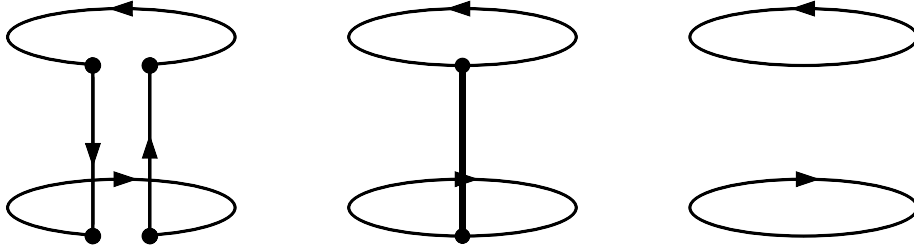


Figure 7. The picture shows the contours of a non-cyclic (left) and a cyclic Wilson loop (middle). One can see how the cusp points turn into intersection points. The contour of the correlator of two Polyakov loops is shown on the right.

It has been shown in Ref. [14] that the expectation values of Wilson loops with intersections cannot be renormalized by a single multiplicative constant. One has to consider instead sets of associated loops and *loop correlators* that mix under renormalization. By loop correlators we mean the expectation values (vacuum or thermal) of products of individually traced loops. These sets of loops and correlators consist of all possible path-ordering prescriptions for contours that occupy the same points in spacetime and retain the same direction everywhere except at the intersection points.

As an illustration consider the simple case shown in Fig. 8, which consists of a smooth curve intersecting itself once at a single point. Following the curve up to the intersection point, one can either go straight ahead thus following the rest of the contour (left picture in Fig. 8), or make a turn onto the way one has come from, thus splitting the contour into two separate loops (right picture in Fig. 8). Each of the two loops in the right picture, taken on its own, would have a cusp and be renormalizable through a multiplicative constant. However, when considering the product of the loops, there are new divergences coming from diagrams with gluon exchanges between the two loops. These new divergences are renormalized together with the smooth loop in the left picture, for which similar divergences arise at the intersection. More precisely, there exist linear combinations of the two loops shown in Fig. 8 that are finite and involve coefficients depending only on the angle at the intersection point.



Figure 8. The two possible path orderings at the intersection point for a loop with one intersection point. In the figure on the right, the two loops are understood to be touching at the cusp points; the separation has been introduced to make clearer that one is dealing with two separate contours.

In general, a Wilson loop may cross an intersection point several times and the angles at which the different lines enter the intersection point may all be different. In that case, the set of all associated loops is renormalized by a matrix of renormalization constants, which depend only upon the angles at the intersection point. When a loop has more than

one intersection point, then the set of associated loops takes on a tensor-like structure with a renormalization matrix for each intersection point. If there are additional cusps present, then those can be taken care of by multiplicative constants. So the general formula for the renormalized loops is⁶

$$W_{i_1 i_2 \dots i_r}^{(R)} = Z_{i_1 j_1}(\theta_1) Z_{i_2 j_2}(\theta_2) \cdots Z_{i_r j_r}(\theta_r) Z(\varphi_1) Z(\varphi_2) \cdots Z(\varphi_s) W_{j_1 j_2 \dots j_r}. \quad (4.1)$$

Here the indices i_k and j_k label the different possible path-ordering prescriptions at the r intersection points, θ_k denote the sets of angles at those intersection points and φ_l stand for the cusp angles at the s additional points of non differentiability. The loop functions, $W_{j_1 j_2 \dots j_r}$, as well as the renormalized ones, $W_{i_1 i_2 \dots i_r}^{(R)}$, are defined such that there is a colour trace over each closed Wilson line, and each trace is normalized by the number of colours. The trace over closed Wilson loops ensures that all loop functions are gauge invariant. The coupling in $W_{i_1 i_2 \dots i_r}^{(R)}$ is the renormalized coupling. The matrices Z are the renormalization matrices. They are one at leading order in perturbation theory, while the explicit expression at higher orders depends on the adopted subtraction scheme. We will adopt the $\overline{\text{MS}}$ scheme.

Now we want to apply the results of Ref. [14], which we have summarized above, and specifically Eq. (4.1) to the case of the cyclic Wilson loop. Although it may seem that the cyclic Wilson loop has a continuously infinite number of intersection points, namely all the points on the overlapping strings (see the second picture in Fig. 7), we need to care only about the two endpoints, for the Wilson loop contour does not lead to divergences in the other ones. As a consequence, we have four possible path orderings (two for each endpoint) when we consider the possible prescriptions at the intersection points, see Fig. 9. We will label the corresponding loop functions W_{ij} , where i and j can assume the values 0 or 1. These are explicitly given by

$$\begin{aligned} W_{00} &= \left\langle \widetilde{\text{Tr}} \left[U_0 \left(\frac{\mathbf{r}}{2}, -\frac{\mathbf{r}}{2} \right) U_{-\frac{\mathbf{r}}{2}}^\dagger(1/T, 0) U_0^\dagger \left(\frac{\mathbf{r}}{2}, -\frac{\mathbf{r}}{2} \right) U_{\frac{\mathbf{r}}{2}}(1/T, 0) \right] \right\rangle = W_c, \\ W_{01} &= \left\langle \widetilde{\text{Tr}} \left[U_0 \left(\frac{\mathbf{r}}{2}, -\frac{\mathbf{r}}{2} \right) U_0^\dagger \left(\frac{\mathbf{r}}{2}, -\frac{\mathbf{r}}{2} \right) U_{\frac{\mathbf{r}}{2}}(1/T, 0) \right] \widetilde{\text{Tr}} \left[U_{-\frac{\mathbf{r}}{2}}^\dagger(1/T, 0) \right] \right\rangle \\ &= \left\langle \widetilde{\text{Tr}} \left[U_{\frac{\mathbf{r}}{2}}(1/T, 0) \right] \widetilde{\text{Tr}} \left[U_{-\frac{\mathbf{r}}{2}}^\dagger(1/T, 0) \right] \right\rangle \equiv P_c, \\ W_{10} &= \left\langle \widetilde{\text{Tr}} \left[U_0 \left(\frac{\mathbf{r}}{2}, -\frac{\mathbf{r}}{2} \right) U_{-\frac{\mathbf{r}}{2}}^\dagger(1/T, 0) U_0^\dagger \left(\frac{\mathbf{r}}{2}, -\frac{\mathbf{r}}{2} \right) \right] \widetilde{\text{Tr}} \left[U_{\frac{\mathbf{r}}{2}}(1/T, 0) \right] \right\rangle = P_c, \\ W_{11} &= \left\langle \widetilde{\text{Tr}} \left[U_{-\frac{\mathbf{r}}{2}}^\dagger(1/T, 0) \right] \widetilde{\text{Tr}} \left[U_0 \left(\frac{\mathbf{r}}{2}, -\frac{\mathbf{r}}{2} \right) U_0^\dagger \left(\frac{\mathbf{r}}{2}, -\frac{\mathbf{r}}{2} \right) \right] \widetilde{\text{Tr}} \left[U_{\frac{\mathbf{r}}{2}}(1/T, 0) \right] \right\rangle = P_c. \end{aligned} \quad (4.2)$$

We see that the four options give rise to two independent loop functions: the cyclic Wilson loop, $W_c = W_{00}$, and the correlator of two Polyakov loops separated by a distance \mathbf{r} , $P_c = W_{01} = W_{10} = W_{11}$. We will call P_c simply the *Polyakov loop correlator*; its contour is shown in the rightmost picture of Fig. 7.

We can represent W_{ij} by a four component vector $(W_{00}, W_{01}, W_{10}, W_{11})$ that gets renormalized by the tensor product of the two renormalization matrices corresponding

⁶The generalization to loop functions with more intersections performed in [14] relies on the assumption that the divergence structure at an intersection point is completely determined by the local characteristics of the contour at this point. This is certainly the case when for each intersection point there are at most two Wilson lines connecting it to other intersection points. For the cyclic Wilson loop we may therefore use Eq. (4.1), although it may not be applicable for more general loop functions.

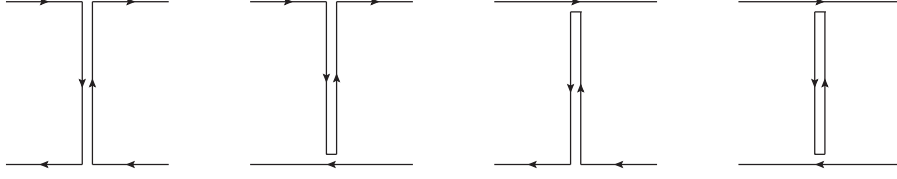


Figure 9. The four different path orderings of the contour of the cyclic Wilson loop that correspond from left to right to the loop functions W_{00} , W_{01} , W_{10} and W_{11} respectively. The strings are represented by the middle lines.

to the two endpoints. Since the angles at both ends of the string are equal, also the renormalization matrices are equal. The renormalization equation reads

$$\begin{pmatrix} W_c^{(R)} \\ P_c^{(R)} \\ P_c^{(R)} \\ P_c^{(R)} \end{pmatrix} = \begin{pmatrix} Z_{00} \begin{pmatrix} Z_{00} & Z_{01} \\ Z_{10} & Z_{11} \end{pmatrix} & Z_{01} \begin{pmatrix} Z_{00} & Z_{01} \\ Z_{10} & Z_{11} \end{pmatrix} \\ Z_{10} \begin{pmatrix} Z_{00} & Z_{01} \\ Z_{10} & Z_{11} \end{pmatrix} & Z_{11} \begin{pmatrix} Z_{00} & Z_{01} \\ Z_{10} & Z_{11} \end{pmatrix} \end{pmatrix} \begin{pmatrix} W_c \\ P_c \\ P_c \\ P_c \end{pmatrix}. \quad (4.3)$$

Since the Polyakov loop correlator is finite, having neither cusps nor intersections, it holds that $P_c^{(R)} = P_c$. From this it follows that Z_{10} has to be zero, otherwise $P_c^{(R)}$ would depend on W_c :

$$\begin{pmatrix} W_c^{(R)} \\ P_c \\ P_c \\ P_c \end{pmatrix} = \begin{pmatrix} Z_{00}^2 & Z_{00}Z_{01} & Z_{00}Z_{01} & Z_{01}^2 \\ 0 & Z_{00}Z_{11} & 0 & Z_{01}Z_{11} \\ 0 & 0 & Z_{00}Z_{11} & Z_{01}Z_{11} \\ 0 & 0 & 0 & Z_{11}^2 \end{pmatrix} \begin{pmatrix} W_c \\ P_c \\ P_c \\ P_c \end{pmatrix}. \quad (4.4)$$

The three equations involving P_c furthermore require $Z_{11} = 1$ and $Z_{01} = 1 - Z_{00}$, which leaves only one independent renormalization constant $Z \equiv Z_{00}^2$. So the renormalization condition for the cyclic Wilson loop and the Polyakov loop correlator reads

$$\begin{pmatrix} W_c^{(R)} \\ P_c \end{pmatrix} = \begin{pmatrix} Z & (1 - Z) \\ 0 & 1 \end{pmatrix} \begin{pmatrix} W_c \\ P_c \end{pmatrix}. \quad (4.5)$$

We will now determine Z .⁷ For the purpose of determining Z at $\mathcal{O}(\alpha_s)$, we just need to know that $P_c = 1 + \mathcal{O}(g^3)$. However, for the forthcoming analysis of Sec. 5, we will need P_c at $\mathcal{O}(\alpha_s^2)$, which we give here. The expectation value of the Polyakov loop correlator is equal to the square of a single Polyakov loop, P_L , plus diagrams involving gluon exchanges between both loops. The one-gluon exchange diagram vanishes, because it is proportional to $(\text{Tr}[T^a])^2 = 0$, so the first contribution comes from the exchange of two gluons [19, 27]. The result at $\mathcal{O}(\alpha_s^2)$ for the same hierarchy of energy scales that we are assuming here, i.e. $1/r \gg T \gg m_D \gg \alpha_s/r$, can be read from [20] or extracted in the appropriate limit from [19, 27, 28]. The Polyakov loop $P_L = 1 + \delta P_L$ has been computed in [9, 20]. The full

⁷ Note that the renormalization constant Z is gauge independent for it relates gauge independent quantities.

$\mathcal{O}(\alpha_s^2)$ result reads

$$P_c = 1 - \left(C_F^2 - \frac{1}{2} C_F C_A \right) \frac{\alpha_s^2}{2r^2 T^2} + 2\delta P_L, \quad (4.6)$$

$$\delta P_L = \frac{C_F \alpha_s m_D}{2T} + C_F \alpha_s^2 \left[C_A \left(\frac{1}{4} + \ln \frac{m_D}{T} \right) - \frac{n_f}{2} \ln 2 \right], \quad (4.7)$$

where $m_D^2 = \frac{g^2 T^2}{3} \left(C_A + \frac{n_f}{2} \right)$.

Let us now apply the renormalization equation (4.5) to the unrenormalized result (3.5). It is convenient to expand Z in powers of α_s (understood as the 2ε -dimensional coupling of dimensional regularization):

$$Z = 1 + Z_1 \alpha_s \mu^{-2\varepsilon} + Z_2 (\alpha_s \mu^{-2\varepsilon})^2 + \mathcal{O}(\alpha_s^3), \quad (4.8)$$

where μ is the scale of dimensional regularization. To the purpose of fixing Z at order α_s , i.e. finding Z_1 , it is sufficient to write Eq. (4.5) as

$$\begin{aligned} W_c^{(R)} &= Z W_c + (1 - Z) P_c \\ &= 1 + \frac{C_F \alpha_s(\mu)}{rT} + \frac{4\pi C_F \alpha_s}{T} \int \frac{d^d k}{(2\pi)^d} \frac{e^{-i\mathbf{r}\cdot\mathbf{k}}}{\mathbf{k}^2} \left(\frac{C_A \alpha_s}{\pi\varepsilon} + Z_1 \alpha_s \right) + \dots, \end{aligned} \quad (4.9)$$

where the coupling is now the renormalized strong-coupling constant in the $\overline{\text{MS}}$ scheme and the dots stand either for finite terms at order α_s^2 or for terms of higher order. Because $W_c^{(R)}$ is finite, Eq. (4.9) fixes Z_1 ; in the $\overline{\text{MS}}$ scheme it reads

$$Z_1 = -\frac{C_A}{\pi} \left(\frac{1}{\varepsilon} - \gamma_E + \ln 4\pi \right) = -\frac{C_A}{\pi} \frac{1}{\bar{\varepsilon}}, \quad (4.10)$$

where, for further use, we have defined $1/\bar{\varepsilon} \equiv 1/\varepsilon - \gamma_E + \ln 4\pi$.

After having removed the divergence from (4.9) according to (4.10), we can perform the Fourier transform of $1/\mathbf{k}^2$ in three dimensions, which gives $1/(4\pi r)$, and write the final expression for the renormalized cyclic Wilson loop in the $\overline{\text{MS}}$ scheme:

$$\begin{aligned} \ln W_c^{(R)} &= \frac{C_F \alpha_s(\mu)}{rT} \left\{ 1 + \frac{\alpha_s}{4\pi} \left[\left(\frac{31}{9} C_A - \frac{10}{9} n_f \right) + \beta_0 (\ln \mu^2 r^2 + 2\gamma_E) \right] \right. \\ &\quad \left. + \frac{\alpha_s C_A}{\pi} \left[1 + 2\gamma_E - 2 \ln 2 + \ln \mu^2 r^2 + \sum_{n=1}^{\infty} \frac{2(-1)^n \zeta(2n)}{n(4n^2 - 1)} (rT)^{2n} \right] \right\} \\ &\quad + \frac{4\pi \alpha_s C_F}{T} \int \frac{d^3 k}{(2\pi)^3} (e^{i\mathbf{r}\cdot\mathbf{k}} - 1) \left[\frac{1}{\mathbf{k}^2 + \Pi_{00}^{(T)}(0, \mathbf{k})} - \frac{1}{\mathbf{k}^2} \right] + C_F C_A \alpha_s^2 + \mathcal{O}(g^5). \end{aligned} \quad (4.11)$$

The above expression is UV finite, the divergences having been reabsorbed either by the renormalization of the strong-coupling constant or by the subtraction of the intersection divergences along Eq. (4.5).

4.1 The cyclic Wilson loop at short distances at leading logarithmic accuracy

Equation (4.11) is accurate up to next-to-leading order (NLO). It contains, however, logarithms in the renormalization scale μ that may be potentially large. These logarithms can be resummed by solving the renormalization group equations for $W_c^{(R)}$, which follow from the renormalization equation (4.5):

$$\begin{cases} \mu \frac{d}{d\mu} (W_c^{(R)} - P_c) = \gamma (W_c^{(R)} - P_c) \\ \mu \frac{d}{d\mu} \alpha_s = -\frac{\alpha_s^2}{2\pi} \beta_0 \end{cases} . \quad (4.12)$$

The renormalized coupling and the loop functions depend on the renormalization scale μ ; the factor γ ,

$$\gamma \equiv \frac{1}{Z} \mu \frac{d}{d\mu} Z = 2C_A \frac{\alpha_s}{\pi} + \mathcal{O}(\alpha_s^2), \quad (4.13)$$

is the anomalous dimension of the operator $W_c^{(R)} - P_c$. The solution of the renormalization group equation is trivial and reads

$$(W_c^{(R)} - P_c)(\mu) = (W_c^{(R)} - P_c)(1/r) \left(\frac{\alpha_s(\mu)}{\alpha_s(1/r)} \right)^{-4C_A/\beta_0}, \quad (4.14)$$

where we have made explicit the normalization scale dependence of $W_c^{(R)} - P_c$. Equation (4.14) implies that $\ln W_c^{(R)}$ in the $\overline{\text{MS}}$ scheme at the scale μ may be written at NLO and leading logarithmic (LL) accuracy (i.e. including all terms of the type $\alpha_s/(rT) \times (\alpha_s \ln \mu r)^n$) as

$$\begin{aligned} \ln W_c^{(R)} = & \frac{C_F \alpha_s(1/r)}{rT} \left\{ 1 + \frac{\alpha_s}{4\pi} \left[\left(\frac{31}{9} C_A - \frac{10}{9} n_f \right) + 2\beta_0 \gamma_E \right] \right. \\ & \left. + \frac{\alpha_s C_A}{\pi} \left[1 + 2\gamma_E - 2 \ln 2 + \sum_{n=1}^{\infty} \frac{2(-1)^n \zeta(2n)}{n(4n^2 - 1)} (rT)^{2n} \right] \right\} \\ & + \frac{4\pi \alpha_s C_F}{T} \int \frac{d^3 k}{(2\pi)^3} (e^{i\mathbf{r} \cdot \mathbf{k}} - 1) \left[\frac{1}{\mathbf{k}^2 + \Pi_{00}^{(T)}(0, \mathbf{k})} - \frac{1}{\mathbf{k}^2} \right] + C_F C_A \alpha_s^2 \\ & + \frac{C_F \alpha_s}{rT} \left[\left(\frac{\alpha_s(\mu)}{\alpha_s(1/r)} \right)^{-4C_A/\beta_0} - 1 \right] + \mathcal{O}(g^5). \end{aligned} \quad (4.15)$$

5 Renormalization up to $\mathcal{O}(\alpha_s^3)$

The renormalization of the cyclic Wilson loop at $\mathcal{O}(\alpha_s^2)$ fixes the renormalization coefficient Z_1 , and only uses the fact that the Polyakov-loop correlator is $1 + \mathcal{O}(g^3)$. In order to provide a nontrivial check of the renormalization equation, we will consider now the renormalization of the cyclic Wilson loop at $\mathcal{O}(\alpha_s^3)$. At that order the expression (4.6) of the Polyakov loop correlator really matters. We will not attempt to compute the full expression of the cyclic Wilson loop at $\mathcal{O}(\alpha_s^3)$, but we will just focus on its divergent contributions and on how

they are renormalized. For this purpose, we will start with a short discussion about the different types of divergences and their origin. We will summarize here the more detailed analyses found in Refs. [11] and [14]. Then we will focus on intersection divergences. In this section, if not otherwise stated, we will not rely on a specific gauge choice.

5.1 Divergences

Ultraviolet divergences come in general from integration regions in position space where two or more vertices are contracted to one point. In the case of internal vertices, one gets the usual divergences removed through charge renormalization. But for loop functions such as the cyclic Wilson loop, one also gets divergences from the contraction of line vertices along the contour. By contractions we mean only those that happen without moving vertices on a quark line to a string line or viceversa, and without altering the contour ordering of the vertices. So, for instance, in a diagram with one vertex on a quark line and two on the opposite, only the latter two can be contracted at the same point, either singular or smooth. For a generic diagram one has a superficial degree of divergence

$$\omega = 1 - N_{\text{ex}}, \quad (5.1)$$

at a smooth point (where the contour is differentiable and non-intersecting), and

$$\omega = -N_{\text{ex}}, \quad (5.2)$$

at a singular point (cusp or intersection); N_{ex} stands for the number of propagators connecting the contraction point to uncontracted vertices.⁸ There are therefore three possible situations that may lead to divergences related to line vertices:

- (1) all vertices are contracted to a smooth point, which leads to a linear divergence;
- (2) the contraction of vertices to a smooth point leaves an external propagator connecting a contracted to an uncontracted vertex: this leads to a logarithmic divergence that we will call *line vertex divergence*;
- (3) all vertices are contracted to a singular point, which gives a logarithmically divergent contribution; these are either *cusp* or *intersection divergences*.

⁸ The gluon propagator satisfies the periodic boundary condition: $D_{\mu\nu}(0, \mathbf{x}) = D_{\mu\nu}(1/T, \mathbf{x})$. In the time interval $0 \leq \tau < 1/T$ the thermal part of $D_{\mu\nu}(\tau, \mathbf{x})$ does not contribute to UV divergences, whereas these follow straightforwardly from considering the vacuum part of $D_{\mu\nu}(\tau, \mathbf{x})$, for instance, in a covariant gauge ξ ,

$$D_{\mu\nu}(x) = \frac{\Gamma(D/2 - 1)}{4\pi^{D/2}} (x^2)^{1-\frac{D}{2}} \left[\frac{1+\xi}{2} \delta_{\mu\nu} + (1-\xi) \left(\frac{D}{2} - 1 \right) \frac{x_\mu x_\nu}{x^2} \right],$$

where $D = 4 - 2\varepsilon$ is the number of dimensions. The counting rules (5.1) and (5.2) apply to covariant gauges. They also apply to the Coulomb gauge, where, however, some diagrams that would be divergent in a covariant gauge vanish (e.g. the first two in the last row of Fig. 6). The counting rules do not apply in general to singular gauges, where diagrams may exhibit a higher superficial degree of divergence. Since we are dealing with gauge-invariant quantities, we are allowed to exclude the case of singular gauges from our considerations.

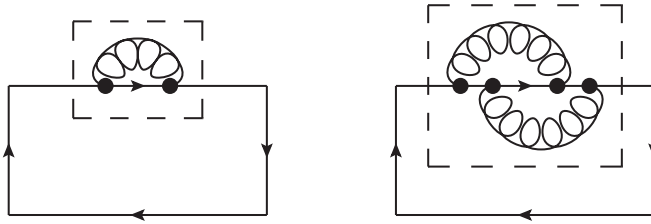


Figure 10. Examples of linear divergences. The divergences arise when the vertices inside the dashed box are contracted to one point.

Linear divergences are proportional to the length of the contour and can be removed by a factor that can be interpreted as a mass term; dimensional regularization removes these power-like divergences automatically [10]. Examples of diagrams with linear divergences are given in Fig. 10. In the notation adopted here, which follows the one in Ref. [14], the dashed box stands for integration regions where all vertices inside the box are contracted to one point. If the box includes a singular point, then the vertices are contracted to that point, otherwise they can be contracted anywhere inside the box.

Line vertex divergences can be removed by using renormalized fields and couplings [11]. Cusp divergences arise from diagrams and integration regions as those depicted in Fig. 11. The one-loop divergence has been given in Eq. (3.6) as a function of the cusp angle γ . From it the renormalization constant for a non-cyclic Wilson loop (i.e. a Wilson loop with a time extension smaller than $1/T$) with four right-angled cusps can be inferred to be in the $\overline{\text{MS}}$ -scheme $Z = \exp[-2C_F\alpha_s\mu^{-2\epsilon}/(\pi\bar{\epsilon})]$. Cusp divergences are absent in a cyclic Wilson loop.

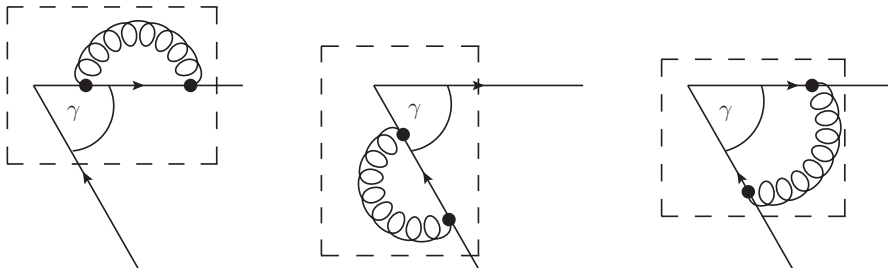


Figure 11. Contributions to a cusp divergence at $\mathcal{O}(\alpha_s)$.

We turn now to the intersection divergences of the cyclic Wilson loop, which are our main point of interest. They only appear when all vertices of a diagram or subdiagram are contracted to an intersection point. In all cases where at least one vertex is on the string, if every vertex of the diagram can be contracted to the intersection, then the contribution of the diagram cancels because of cyclicity. If all vertices are on a quark line, then the diagram contributes equally to the Polyakov loop, which is finite after charge renormalization. This leads to the conclusion that a connected diagram cannot give rise to an intersection divergence, because either all vertices can be contracted to an intersection point, in which case either the divergence cancels because of cyclicity or because it contributes to the

Polyakov loop, or it has at least one uncontracted vertex and therefore it is finite according to Eq. (5.2). These different possibilities correspond to the three diagrams in the first row of Fig. 12. The first diagram has line vertices only on one quark line, so it also contributes to the Polyakov loop, which is finite. The second diagram has vertices on a string and on one quark line and thus cancels through cyclicity. The third diagram involves both quark lines, which means that the line vertices cannot be contracted to the same intersection point and therefore this diagram is finite according to (5.2). This exhausts all possible types of connected diagrams.

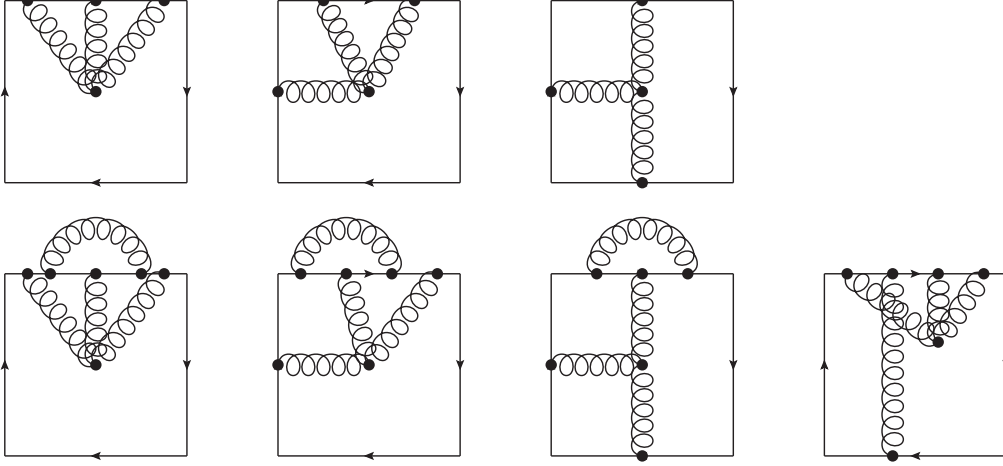


Figure 12. The diagrams in the top row are connected and do not contribute to intersection divergences: they either cancel through cyclicity or contribute to the Polyakov loop. Conversely, some of the unconnected diagrams in the bottom row may show intersection divergences. See the text for details.

Intersection divergences in a cyclic Wilson loop come from unconnected diagrams.⁹ In particular they come from unconnected diagrams made of at least one subdiagram with vertices on both quark lines and a subdiagram that is divergent once all its vertices are contracted to an intersection point. This can be understood by looking at the Feynman diagrams in the second row of Fig. 12. The first diagram is part of the Polyakov loop, which is finite, the second diagram cancels because of cyclicity, but the third and fourth diagrams are divergent, because we can contract the line vertices of the respective one-gluon and three-gluon subdiagrams to an intersection point. The periodic boundary conditions are of crucial importance here, because in order to have no external lines, the intersection point must be approached from the left and the right, as depicted in Fig. 13.

As we just argued, diagrams contributing to intersection divergences need to contain at least one subdiagram with vertices on both quark lines. We call such subdiagrams *bases*. To be more specific, for each intersection-divergent diagram we define its basis as the subdiagram which is of highest order in α_s and still finite. In other words, the basis of a diagram is the subdiagram which is obtained by removing all parts that contribute to the divergence, but no more than that. Conversely, we can obtain all intersection-divergent

⁹ Equation (2.6) allows us to restrict to 2PI unconnected diagrams.

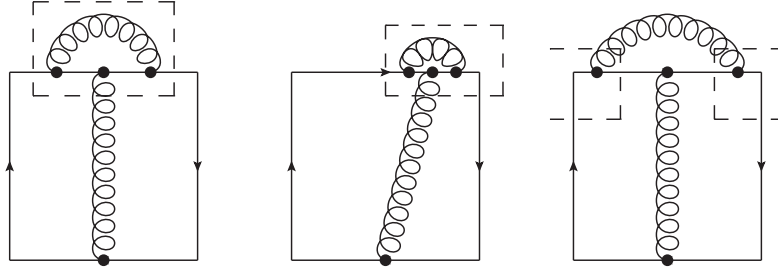


Figure 13. Intersection divergences of subdiagrams. If the line vertices are contracted as in the left (to a smooth point) and middle diagram (to a singular point), we get respectively a line vertex divergence or a finite contribution because of the external line. But the periodic boundary conditions also allow for a contraction to a singular point without external lines, as shown by the right diagram.

diagrams by considering all possible bases and combining them with all subdiagrams that lead to an intersection divergence. This classification of the intersection-divergent diagrams according to their bases and intersection-divergent subdiagrams provides the framework for the following analysis.

All bases relevant for the computation of intersection divergences at $\mathcal{O}(\alpha_s^3)$ are given by the eight diagrams shown in Fig. 14. Note that bases may be reducible, provided that adding intersection-divergent subdiagrams makes them 2PI. In order to get all diagrams contributing to intersection divergences at this order, we need to add subdiagrams of $\mathcal{O}(\alpha_s^2)$ to the first basis, and a single gluon exchange to the other bases, in such a way that their line vertices can be contracted to at least one of the intersection points.

The obtained diagrams may be divided into *classes*. A class of diagrams is made of diagrams that have the same basis and that can be transformed one into the other by just moving some of the line vertices across the intersection point from string to quark line or from quark line to string without changing their ordering along the contour of the Wilson loop. A class of $\mathcal{O}(\alpha_s^2)$ diagrams is shown in Fig. 15; a class will be typically represented by just one of its diagrams.

5.2 Renormalization

We consider first the effect of a single gluon when added to one of the diagrams in Fig. 14. It generates two classes of diagrams that lead to intersection divergences: one is shown in Fig. 16 with an intersection divergence at $\mathbf{r}/2$, the other one would have the gluon attached to the lower quark like and an intersection divergence at $-\mathbf{r}/2$. In Fig. 16, the contour integration for the left vertex of the gluon goes from $(0, \mathbf{cr})$ to $(a/T, \mathbf{r}/2)$, and the contour integration for the right vertex goes from $(-(1-b)/T, \mathbf{r}/2)$ to $(0, \mathbf{dr})$, where we have used the periodic boundary conditions to shift the right vertex by $-1/T$ in time; the grey area stands for a generic basis. Colour factors are considered separately. In a generic covariant

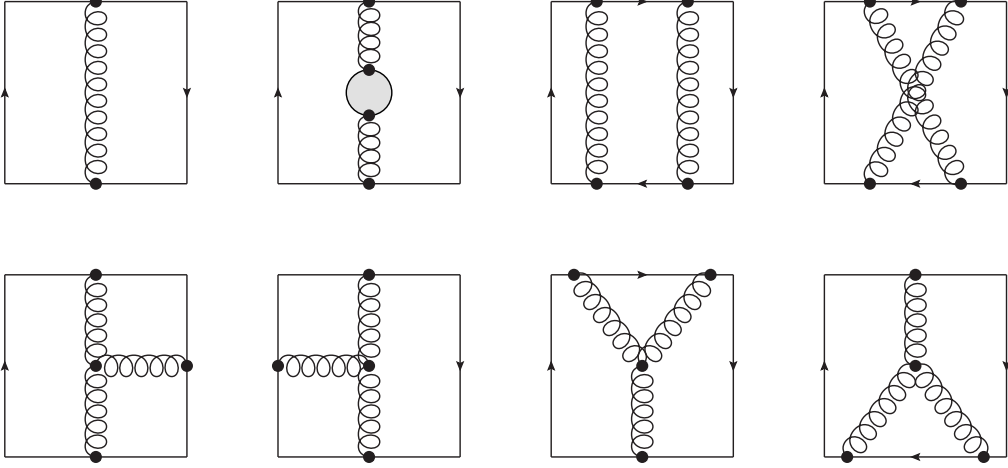


Figure 14. Bases relevant for the intersection divergences of $\mathcal{O}(\alpha_s^3)$.

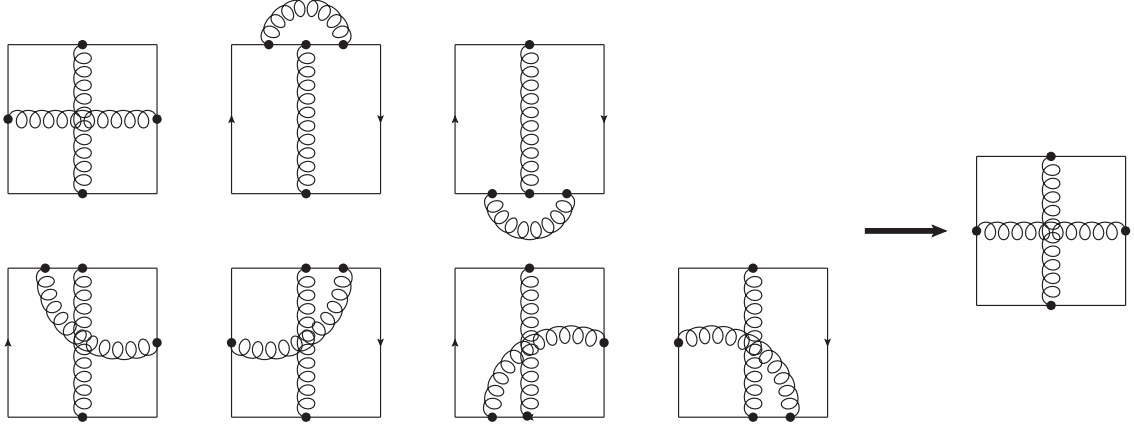


Figure 15. A class of 2PI diagrams represented by the diagram on the right. In Coulomb gauge the diagram on the right is the only one that does not vanish, see Sec. 3.

gauge, the result reads:

$$\begin{aligned}
& -\frac{\alpha_s}{\pi} \left[\frac{1}{\varepsilon} + 2\gamma_E - \ln 4 + 2 + \ln \frac{\mu a(1-b)}{T(1-b+a)} + \ln \frac{(\frac{1}{2}-c)(\frac{1}{2}-d)}{|c-d|} r\mu \right. \\
& \left. + \frac{1}{2}(1-\xi) \ln \frac{\sqrt{(\frac{1}{2}-d)^2 r^2 T^2 + a^2} \sqrt{(\frac{1}{2}-c)^2 r^2 T^2 + (1-b)^2}}{(1-b+a)|c-d| r T} \right]. \quad (5.3)
\end{aligned}$$

The divergent part does not depend on the contour parameters a, b, c, d , hence, it can be factored out from the contour integration. Because the contour parameters only appear in logarithms, they do not introduce new divergences when the contour integration for the basis is performed, since the basis is by definition free from intersection divergences. The fact that the divergence factorizes can be intuitively understood by noting that it comes from integration regions where all vertices of the added subdiagram are at the intersection,

so it is unaffected by the contour integration for the basis (see also Ref. [14]). Note that the divergent part of (5.3), i.e. $-\alpha_s/\pi \times 1/\bar{\epsilon}$, does not depend on the gauge fixing parameter ξ ; furthermore, the same divergent part occurs also in Coulomb gauge, in which case, however, only the integration along the strings contributes. The second class of diagrams with the gluon attached to the lower quark line gives the same divergence as in (5.3).

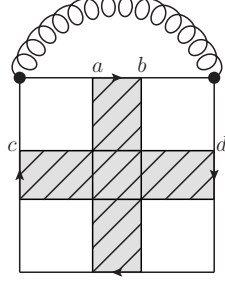


Figure 16. Class of diagrams with a one-gluon subdiagram.

At order $\mathcal{O}(\alpha_s^2)$ the only class of divergent diagrams is shown in Fig. 15. The divergence of that class is $\tilde{C}_2 \times 2 \times (-\alpha_s/\pi \times 1/\bar{\epsilon}) \times (\text{basis, i.e. the one-gluon exchange diagram, } \alpha_s/r)$; \tilde{C}_2 is the colour-connected coefficient of the diagrams, the factor 2 comes from the two intersection divergences at $\mathbf{r}/2$ and $-\mathbf{r}/2$, and the divergence is the one calculated in (5.3). The cancellation of this divergence in the $\overline{\text{MS}}$ -scheme fixes Z_1 to the value calculated in (4.10).

Both W_c and P_c are equal to 1 at zeroth order in α_s . At that order the renormalization condition is automatically fulfilled: $Z + (1 - Z) = 1$. A similar cancellation happens at any order (including odd powers of g from contributions of the Debye mass scale) when the renormalization constant multiplies diagrams that occur identically in both the cyclic Wilson loop and the Polyakov loop correlator. These are contributions to the cyclic Wilson loop coming from the gluon self-energy diagrams in the top row of Fig. 6 (second and third diagram) and from the diagrams in the bottom row of Fig. 6 (third and fourth diagram), and the contribution to the Polyakov loop correlator coming from the Polyakov loop, which is $P_L^2 - 1 \approx 2\delta P_L$ in Eq. (4.6). An example of cancellation is shown in Fig. 17.

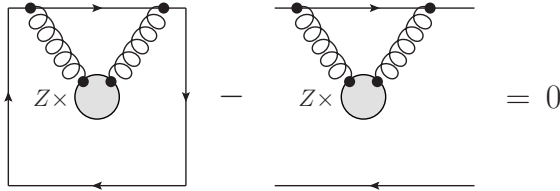


Figure 17. Cancellation of contributions from W_c and P_c . The Polyakov-loop correlator is represented without strings.

Let us discuss now divergences coming from $\mathcal{O}(\alpha_s^3)$ unconnected diagrams in the cyclic Wilson loop. We start by considering classes of diagrams whose basis is the second diagram in the first row of Fig. 14. The cancellation of the divergences carried by these diagrams

in the renormalization equation is a simple extension of the cancellation that happens at $\mathcal{O}(\alpha_s^2)$ between the intersection divergence carried by the last diagram of the second row of Fig. 6 and $Z_1\alpha_s$ times the one-gluon exchange diagram. This is illustrated in Fig. 18, where the bubble stands for any self-energy insertion. Also in this case, odd powers of g coming from the Debye mass scale, such as a term arising at order g^5 in our adopted hierarchy of energy scales, cancel out.

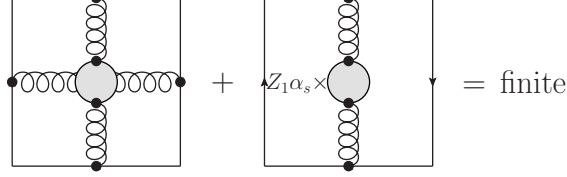


Figure 18. The divergences of the two classes of diagrams cancel for the same reason as the lower-order classes of diagrams without self-energy insertions do. The gluon connecting the strings does not interact with the bubble.

The cancellation of divergences carried by classes of diagrams whose bases are from the second row of Fig. 14 (shown in Fig. 19), which we will call collectively γ_T , is similar to the one discussed in the previous paragraph. They are cancelled by $Z_1\alpha_s$ times the respective basis diagram from the $\mathcal{O}(\alpha_s^2)$ expansion of W_c . As shown by Eq. (5.3) and the following discussion, adding one gluon to a basis gives a divergent factor, which is $2 \times (-\alpha_s/(\pi\bar{\epsilon}))$. The colour factor of the bases is $iC_F C_A/2$, the colour-connected coefficient of diagrams like those in Fig. 19 is $-iC_F C_A^2/4$. With this it is easy to see that the divergence of a class of diagrams with basis γ_T is:

$$\left(-\frac{2\alpha_s}{\pi\bar{\epsilon}}\right) \left(-\frac{i}{4}C_F C_A^2\right) W(\gamma_T) = -Z_1\alpha_s \left(\frac{i}{2}C_F C_A\right) W(\gamma_T), \quad (5.4)$$

where $W(\gamma_T)$ denotes the value of a diagram belonging to γ_T without its colour factor. We see that all these divergences cancel in ZW_c at $\mathcal{O}(\alpha_s^3)$.

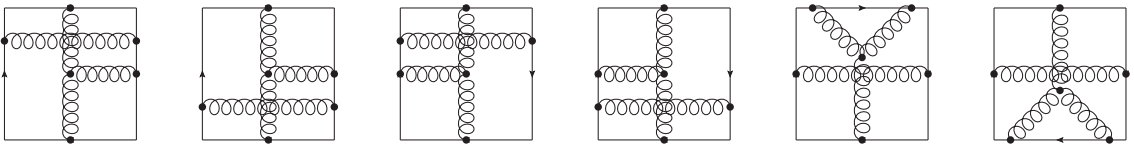


Figure 19. Classes of diagrams with an intersection divergence and a three-gluon diagram as basis.

With the cancellation of divergences associated to classes of diagrams whose basis is either the third or fourth diagram in the first row of Fig. 14, we come to the first non-trivial check of the renormalization equation (4.5). We call the basis with two ladder gluons (i.e. the third diagram in the first row of Fig. 14), γ_{II} , and the one with two crossed gluons (i.e. the fourth diagram in the first row of Fig. 14), γ_X . Without colour factors the sum of these two bases gives just half of the square of the $\mathcal{O}(\alpha_s)$ diagram, so $W(\gamma_{II}) + W(\gamma_X) = \alpha_s^2/(2r^2 T^2)$. The colour-connected coefficients for the diagrams

with γ_{II} and γ_X as bases (these are the diagrams (d) and (e) of Fig. 20) are $C_F C_A^2/4$ and $C_F C_A^2/2$ respectively. The divergences associated to these classes of diagrams are of the type of Fig. 16 and bring a factor $-\alpha_s/\pi \times 1/\bar{\epsilon}$ for each intersection point. In order to cancel these divergences, we have to collect also divergences coming from $Z_1 \alpha_s \times W_c$ that are not of the type cancelled by the Polyakov loop and divergences coming from the expansion of the exponential on the right-hand side of Eq. (2.6) (recall that the exponent is made by 2PI diagrams only). We will highlight only the divergent terms and use the symbol “ \supset ” with the meaning “includes the divergent term”. We have (compare with Fig. 20):

- (a) the renormalization constant $Z_1 \alpha_s$ multiplying the second order expansion term of the one-gluon exchange diagram: $Z_1 \alpha_s \times W_c \supset \left(-\frac{C_A \alpha_s}{\pi \bar{\epsilon}}\right) \times \frac{1}{2} \left(\frac{C_F \alpha_s}{rT}\right)^2$;
- (b) the renormalization constant $Z_1 \alpha_s$ multiplying the basis γ_X (whose colour-connected coefficient is $\tilde{C}_2 = -C_F C_A/2$): $Z_1 \alpha_s \times W_c \supset \left(-\frac{C_A \alpha_s}{\pi \bar{\epsilon}}\right) \times \left(-\frac{C_F C_A}{2} W(\gamma_X)\right)$;
- (c) the one-gluon exchange diagram times the intersection-divergent diagrams at $\mathcal{O}(\alpha_s^2)$ from the expansion of the exponential: $W_c \supset \left(\frac{C_F \alpha_s}{rT}\right) \times \left(\frac{C_A \alpha_s}{\pi \bar{\epsilon}}\right) \left(\frac{C_F \alpha_s}{rT}\right)$;
- (d) + (e) the divergent contributions from diagrams with bases γ_{II} and γ_X :
 $W_c \supset \left(-\frac{2\alpha_s}{\pi \bar{\epsilon}}\right) \left[\frac{1}{4} C_F C_A^2 W(\gamma_{II}) + \frac{1}{2} C_F C_A^2 W(\gamma_X)\right]$.

Summing up these contributions, we get

$$\begin{aligned} ZW_c &\supset \left(-\frac{C_F C_A^2 \alpha_s}{2\pi \bar{\epsilon}}\right) [W(\gamma_{II}) + 2W(\gamma_X) - W(\gamma_X)] - \frac{C_F^2 \alpha_s^2}{2r^2 T^2} \frac{C_A \alpha_s}{\pi \bar{\epsilon}} + \frac{C_F^2 \alpha_s^2}{r^2 T^2} \frac{C_A \alpha_s}{\pi \bar{\epsilon}} \\ &= \left(C_F^2 - \frac{1}{2} C_F C_A\right) \frac{\alpha_s^2}{2r^2 T^2} \frac{C_A \alpha_s}{\pi \bar{\epsilon}}. \end{aligned} \quad (5.5)$$

This is exactly cancelled by the remaining contributions coming from the Polyakov loop correlator (4.6), given as (f) + (g) in Fig. 20:

$$(1 - Z)P_c \supset \frac{C_A \alpha_s}{\pi \bar{\epsilon}} \times \left[-\left(C_F^2 - \frac{1}{2} C_F C_A\right) \frac{\alpha_s^2}{2r^2 T^2}\right]. \quad (5.6)$$

The cancellation provides a non-trivial verification of the renormalization equation (4.5). Note that the cancellation of the diagrams in Fig. 20 is gauge independent, since Z_1 , the one-gluon exchange diagram, the Polyakov-loop correlator as well as the combination $W(\gamma_{II}) + W(\gamma_X)$ are gauge invariant.

Finally, we observe that the second-order expansion term of the renormalization constant times $\mathcal{O}(\alpha_s)$ diagrams of the cyclic Wilson loop gives a divergent term like

$$ZW_c \supset Z_2 \alpha_s^2 \times \frac{C_F \alpha_s}{rT}, \quad (5.7)$$

where Z_2 may contain single or double poles in $1/\bar{\epsilon}$. This term is necessary to cancel divergent contributions coming from unconnected diagrams that have the one-gluon exchange

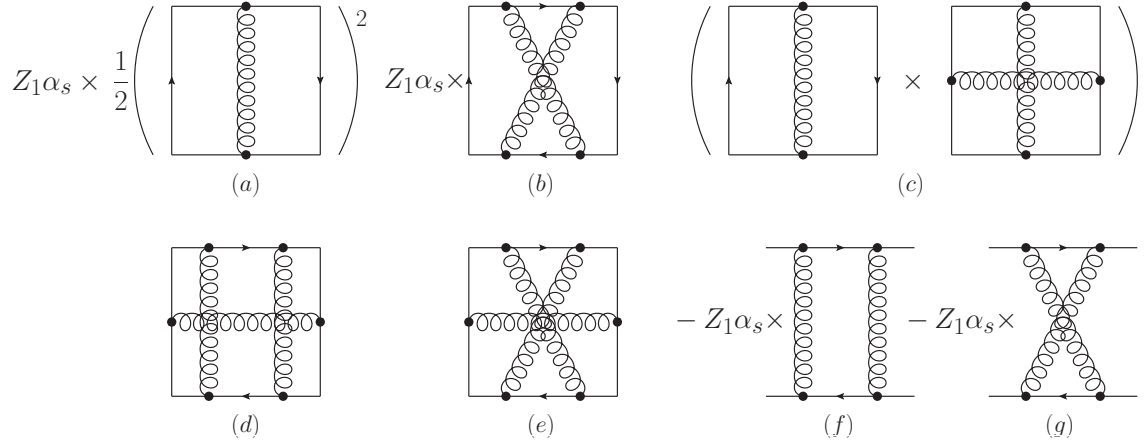


Figure 20. The sum of all these contributions is finite. It includes all diagrams with bases made of two gluons exchanged between the quark lines, and related contributions from both the cyclic Wilson loop and the Polyakov loop correlator (diagrams (f) and (g)).

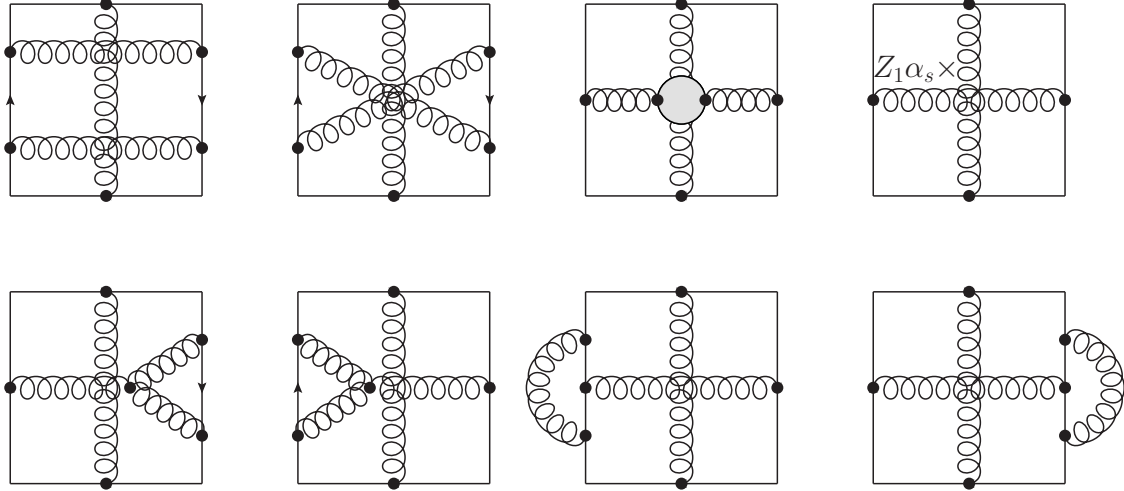


Figure 21. Classes of diagrams contributing to Z_2 .

diagram, i.e. the first diagram of Fig. 14, as a basis and subdiagrams of $\mathcal{O}(\alpha_s^2)$ added. The different diagram classes are shown in Fig. 21. The sum of all divergent terms of these diagrams (after charge renormalization) determines the value of Z_2 .

Because the right-hand side of Eq. (5.7) is proportional to $1/(rT)$, in order to complete our proof of renormalizability at $\mathcal{O}(\alpha_s^3)$ we have to make sure that the sum of diagrams in Fig. 21 only contains divergent terms proportional to $1/(rT)$. The second and the third classes of diagrams in the first row and the classes of diagrams in the second row of Fig. 21 do indeed fulfill this criterion. The reason is that, in order to get an intersection divergence from these diagrams, we have to contract all gluons but the one connecting the two quark lines to the intersection points, otherwise there would be a gluon propagator connecting the intersection point with an uncontracted vertex and from Eq. (5.2) we know that such a con-

figuration is convergent. As a consequence, since the divergence at the contraction does not depend on r , the complete r dependence comes from the one-gluon exchange, which is proportional to $1/(rT)$. The same reasoning applies to the first and fourth classes of diagrams in the first row if we contract all gluons but the one connecting the two quark lines to the intersection points. Such kind of intersection divergence is called *overall divergence* in [14], to distinguish it from a *subdivergence*, which is a divergence that occurs when only one of the gluons is contracted to the intersection points. Consider the first diagram in Fig. 21. Its colour-connected coefficient is $C_F C_A^2/4$ just like diagram (d) of Fig. 20. A subdivergence may come either by contracting the upper gluon connecting the strings to the intersection point at $\mathbf{r}/2$ and keeping the finite part of the remaining diagram, or by contracting the lower gluon to the intersection point at $-\mathbf{r}/2$ and keeping again the finite part of the remaining diagram. The divergence may be read from (5.3) and is $-\alpha_s/(\pi\bar{\epsilon})$; the finite part is the same for the two situations and we call it $W(\gamma_+)^{(\text{finite})}$. Hence, the subdivergence of the first diagram in Fig. 21 is $\frac{1}{4}C_F C_A^2 \left(-\frac{2\alpha_s}{\pi\bar{\epsilon}}\right) W(\gamma_+)^{(\text{finite})}$. Because $W(\gamma_+)^{(\text{finite})}$ has a more complicate functional dependence than just $1/(rT)$, this is a divergence that is not canceled by the right-hand side of (5.7). Consider now the fourth diagram in Fig. 21 when none of the gluons is contracted to an intersection point. The colour-connected coefficient is $\tilde{C}_2 = -C_F C_A/2$. The divergence is $(Z_1\alpha_s) \times \left(-\frac{1}{2}C_F C_A\right) W(\gamma_+)^{(\text{finite})}$. Note that the finite part is the same multiplying the subdivergence in the first diagram. Summing up the (sub)divergences of the two diagrams we obtain

$$ZW_c \supset \frac{1}{4}C_F C_A^2 \left(-\frac{2\alpha_s}{\pi\bar{\epsilon}}\right) W(\gamma_+)^{(\text{finite})} + \left(-\frac{C_A\alpha_s}{\pi\bar{\epsilon}}\right) \left(-\frac{1}{2}C_F C_A\right) W(\gamma_+)^{(\text{finite})} = 0, \quad (5.8)$$

where we have used the value of Z_1 derived in (4.10). This completes our proof of renormalizability of the intersection divergences at $\mathcal{O}(\alpha_s^3)$.

6 The cyclic Wilson loop at large distances

Equation (4.5) establishes how the cyclic Wilson loop renormalizes, i.e. by mixing with the Polyakov loop correlator. Although we have tested the equation in a specific hierarchy of energy scales, i.e. $1/r \gg T \gg m_D \gg \alpha_s/r$, its validity is not bound to this hierarchy for it follows from general arguments based ultimately only on the UV behaviour of QCD and on the geometry of the loop functions [14]. In particular, Eq. (4.5) should also hold for cyclic Wilson loops at large distances, i.e. for $rm_D \sim 1$.

Let us consider in the long-distance case $rm_D \sim 1$ the UV divergences of the cyclic Wilson loop at $\mathcal{O}(\alpha_s^2)$. To make contact with Sec. 3 we work in Coulomb gauge. The divergent diagram is again the last diagram in the second row of Fig. 6. The divergence comes from the vacuum part of the transverse gluon connecting the two strings. As expected, this quantity is insensitive to the low energy dynamics: the thermal part of the transverse gluon gives a finite contribution, the temperature providing a UV cut-off through the Bose–Einstein distribution, moreover transverse gluons are not screened. The temporal gluon connecting the quark lines is instead screened by the Debye mass. This is the only

difference with the calculation performed in Sec. 3. Because the temporal gluon factorizes, at long distances the leading divergence of the cyclic Wilson loop due to intersection may be easily inferred from Eq. (3.4). Adding to it the leading-order diagram, which consists of the first diagram in Fig. 1, also with a screened temporal gluon, we get

$$W_c = 1 + \frac{4\pi C_F \alpha_s(\mu)}{T} \frac{e^{-m_D r}}{4\pi r} + \frac{4C_F C_A \alpha_s^2}{T} \frac{e^{-m_D r}}{4\pi r} \frac{1}{\varepsilon} + \dots, \quad (6.1)$$

where $\exp(-m_D r)/(4\pi r)$ is the Fourier transform in three dimensions of the screened temporal gluon propagator, $D_{00}(0, \mathbf{k}) = 1/(\mathbf{k}^2 + m_D^2)$, and the dots stand either for finite terms or for terms of higher order. It is straightforward to see that the expression in (6.1) is renormalized by (4.5) with the same renormalization constant Z computed in (4.8) and (4.10). This confirms, at least at leading order, our expectation that Eq. (4.5) renormalizes the cyclic Wilson loop at any distance. Finally, we note that our conclusion and in particular Eq. (6.1) disagree with the long-distance finding of [9].¹⁰

7 Conclusions

We have investigated the UV behaviour of the cyclic Wilson loop. Our short-distance, order- g^4 calculation, summarized in Eq. (3.5), confirms the finding of Ref. [9], namely that the cyclic Wilson loop is divergent after charge renormalization and that its divergence is not a standard cusp divergence.

In Sec. 4, we have shown how the periodic boundary conditions influence the divergences and the renormalization properties of the cyclic Wilson loop. The contour can be seen as having intersection points along the two strings, but only the two endpoints are relevant for renormalization purposes. Applying the intersection-divergence renormalization technique of Ref. [14], we have obtained the renormalization equation for the cyclic Wilson loop: $W_c^{(R)} = ZW_c + (1 - Z)P_c$. This equation represents the main result of the paper and shows how the cyclic Wilson loop, W_c , mixes under renormalization with the correlator of two Polyakov loops, P_c , their mixing being determined by the renormalization constant Z . The equation holds for all $SU(N_c)$ gauge theories; in the case of an abelian gauge theory, the cyclic Wilson loop and the correlator of Polyakov loops coincide and are finite.

¹⁰ The disagreement may be traced back to the contribution from the non-zero modes to the transverse gluon connecting the strings in the last diagram in the second row of Fig. 6. In our computation, the relevant integral reads

$$\sum_{n \neq 0} \int \frac{d^d q}{(2\pi)^d} \frac{(e^{i\mathbf{r} \cdot \mathbf{q}} + e^{-i\mathbf{r} \cdot \mathbf{q}} - 2) r^2}{2(\mathbf{r} \cdot \mathbf{q})^2 (\mathbf{q}^2 + \omega_n^2)} = \frac{1}{8\pi^2 T} \left[\frac{1}{\varepsilon} + \gamma_E - \ln 4\pi + \ln \frac{\mu^2}{T^2} + 2 \int_1^\infty \frac{dx}{x^2} \ln(1 - e^{-2\pi r T x}) \right. \\ \left. + \pi r T \left(\frac{1}{\varepsilon} - \gamma_E + \ln 4\pi + \ln \frac{\mu^2}{T^2} \right) \right].$$

The first line agrees with Eq. (A.19) of [9], but the second line, which comes from the non-vanishing contributions from the double pole at $\mathbf{r} \cdot \mathbf{q} = 0$ in the two half-planes where the two Fourier exponentials separately converge, is missing. It is precisely the $1/\varepsilon$ singularity in the second line that cancels the UV divergence coming from the zero modes, while the singularity in the first line, combined with other contributions, leads eventually to the result (6.1). We thank the authors of [9] for communication on this point.

We have determined the renormalization constant, Z , up to order g^2 , obtaining $Z = 1 - C_A \alpha_s \mu^{-2\varepsilon} / \pi \times (1/\varepsilon - \gamma_E + \ln 4\pi)$ in the $\overline{\text{MS}}$ scheme. In Sec. 5, we have verified that this expression of Z reabsorbs all divergences of the type $\alpha_s^3/(rT)^2$; this is a non-trivial check involving the Polyakov-loop correlator at order α_s^2 . From the renormalization constant we could extract the intersection anomalous dimension at one loop and solve the corresponding renormalization group equations (4.12). The result provides the cyclic Wilson loop at LL accuracy (4.15), which is the novel computational outcome of this work.

Finally, we observe that the renormalization condition (4.5) is equivalent to stating that the combination $W_c - P_c$ is multiplicatively renormalizable.¹¹ The combination $W_c - P_c$ is therefore an ideal quantity to be computed on the lattice, while clearly the cyclic Wilson loop is not (see discussion in [9]). It could provide a new, independent and gauge-invariant lattice observable for the study of the thermodynamical properties of two static sources in a thermal bath, relevant for quarkonium physics in a quark-gluon plasma, being at the same time well suited for comparisons with analytic studies like the one performed in this work.

Acknowledgments

We acknowledge financial support from the DFG cluster of excellence *Origin and structure of the universe* (www.universe-cluster.de). This research is supported by the DFG grant BR 4058/1-1. The work of J.G. was supported by the National Science and Engineering Research Council of Canada and by an Institute of Particle Physics Theory Fellowship. Part of the work of M.B. was done at Kyoto University and supported by the Global Cluster of Excellence (GCOE) in the framework of the Bilateral International Exchange Program (BIEP) of 2012; M.B. thanks Prof. Hideo Suganuma and his group for their warm hospitality.

References

- [1] K. G. Wilson, Phys. Rev. D **10** (1974) 2445.
- [2] L. Susskind, in “Les Houches 1976, Proceedings, Weak and Electromagnetic Interactions At High Energies”, (Amsterdam, 1977), 207.
- [3] L. S. Brown and W. I. Weisberger, Phys. Rev. D **20** (1979) 3239.
- [4] N. Brambilla *et al.*, “Heavy quarkonium physics”, CERN-2005-005, (CERN, Geneva, 2005) [arXiv:hep-ph/0412158].
- [5] N. Brambilla, A. Pineda, J. Soto and A. Vairo, Rev. Mod. Phys. **77** (2005) 1423 [hep-ph/0410047].
- [6] N. Brambilla, S. Eidelman, B. K. Heltsley, R. Vogt, G. T. Bodwin, E. Eichten, A. D. Frawley and A. B. Meyer *et al.*, Eur. Phys. J. C **71** (2011) 1534 [arXiv:1010.5827 [hep-ph]].

¹¹ In dimensional regularization this implies that the ratio $(W_c - P_c)(r)/(W_c - P_c)(r_0)$, where the loop functions in $(W_c - P_c)(r)$ are evaluated at a distance r while those in $(W_c - P_c)(r_0)$ are evaluated at a fixed distance r_0 , is finite. On the lattice, because of linearly divergent renormalization factors proportional to r and $1/T$, a possible finite quantity is $(W_c - P_c)(r)/(W_c - P_c)(r_0) \times (W_c - P_c)(2r_0 - r)/(W_c - P_c)(r_0)$.

- [7] T. Matsui and H. Satz, Phys. Lett. B **178** (1986) 416.
- [8] A. Bazavov, P. Petreczky and A. Velytsky, arXiv:0904.1748 [hep-ph].
- [9] Y. Burnier, M. Laine and M. Vepsalainen, JHEP **1001** (2010) 054 [arXiv:0911.3480 [hep-ph]].
- [10] A. M. Polyakov, Nucl. Phys. B **164** (1980) 171.
- [11] V. S. Dotsenko and S. N. Vergeles, Nucl. Phys. B **169** (1980) 527.
- [12] G. P. Korchemsky and A. V. Radyushkin, Nucl. Phys. B **283** (1987) 342.
- [13] D. Correa, J. Henn, J. Maldacena and A. Sever, JHEP **1205** (2012) 098 [arXiv:1203.1019 [hep-th]].
- [14] R. A. Brandt, F. Neri and M. -a. Sato, Phys. Rev. D **24** (1981) 879.
- [15] M. Berwein, Master’s thesis, TU Munich, (2011).
- [16] R. A. Brandt, A. Gocksch, M. -a. Sato and F. Neri, Phys. Rev. D **26** (1982) 3611.
- [17] J. G. M. Gatheral, Phys. Lett. B **133** (1983) 90.
- [18] J. Frenkel and J. C. Taylor, Nucl. Phys. B **246** (1984) 231.
- [19] L. D. McLerran and B. Svetitsky, Phys. Rev. D **24** (1981) 450.
- [20] N. Brambilla, J. Ghiglieri, P. Petreczky and A. Vairo, Phys. Rev. D **82** (2010) 074019 [arXiv:1007.5172 [hep-ph]].
- [21] U. W. Heinz, K. Kajantie and T. Toimela, Annals Phys. **176** (1987) 218.
- [22] J. I. Kapusta and C. Gale, “Finite-temperature field theory: Principles and applications”, (Cambridge, 2006), 428 p.
- [23] N. Brambilla, J. Ghiglieri, A. Vairo and P. Petreczky, Phys. Rev. D **78** (2008) 014017 [arXiv:0804.0993 [hep-ph]].
- [24] A. Andrasi, Eur. Phys. J. C **37** (2004) 307 [hep-th/0311118].
- [25] W. Fischler, Nucl. Phys. B **129** (1977) 157.
- [26] A. Billoire, Phys. Lett. B **92** (1980) 343.
- [27] D. J. Gross, R. D. Pisarski and L. G. Yaffe, Rev. Mod. Phys. **53** (1981) 43.
- [28] S. Nadkarni, Phys. Rev. D **33** (1986) 3738.